nature neuroscience

RESOURCE

https://doi.org/10.1038/s41593-019-0431-2

Targeting neuronal and glial cell types with synthetic promoter AAVs in mice, non-human primates and humans

Josephine Jüttner[1,2], Arnold Szabo[3], Brigitte Gross-Scherf[1,2], Rei K. Morikawa[1,2], Santiago B. Rompani[1,2,10], Peter Hantz[2,11], Tamas Szikra[1,2], Federico Esposti[2,12], Cameron S. Cowan[1,2], Arjun Bharioke[1,2], Claudia P. Patino-Alvarez[1,2], Özkan Keles[1,2], Akos Kusnyerik[1,4], Thierry Azoulay[5], Dominik Hartl[2], Arnaud R. Krebs[2,13], Dirk Schübeler[2,6], Rozina I. Hajdu[4], Akos Lukats[3], Janos Nemeth[4], Zoltan Z. Nagy[4], Kun-Chao Wu[7], Rong-Han Wu[7], Lue Xiang[7], Xiao-Long Fang[7], Zi-Bing Jin[7], David Goldblum[8], Pascal W. Hasler[8], Hendrik P. N. Scholl[1,8,9], Jacek Krol[1,2*] and Botond Roska[1,2,8*]

Targeting genes to specific neuronal or glial cell types is valuable for both understanding and repairing brain circuits. Adeno-associated viruses (AAVs) are frequently used for gene delivery, but targeting expression to specific cell types is an unsolved problem. We created a library of 230 AAVs, each with a different synthetic promoter designed using four independent strategies. We show that a number of these AAVs specifically target expression to neuronal and glial cell types in the mouse and non-human primate retina in vivo and in the human retina in vitro. We demonstrate applications for recording and stimulation, as well as the intersectional and combinatorial labeling of cell types. These resources and approaches allow economic, fast and efficient cell-type targeting in a variety of species, both for fundamental science and for gene therapy.

The concept of cell types—morphologically, physiologically and molecularly similar groups of neurons within a given brain region—has become an important starting point for understanding and modulating brain function. In basic research, genetic labeling of neuronal or glial cell types enables their isolation and molecular characterization. Genetically encoded sensors or electrical recording aimed at neuronal cell types allow monitoring of activity; optogenetic or chemogenetic tools permit modulation of activity. In translational research, cell-type-targeted modulation of brain function and cell-type-specific gene replacement are repair strategies for treating human diseases.

Despite the central importance for both basic and translational research, most current technologies available for cell-type targeting rely on transgenic animals, which limits their applicability. Either the genetic tool that senses or modulates brain function, or the enzyme, such as Cre recombinase, which allows the genetic tool to be conditionally expressed, is expressed from the animal's genome. Cell-type targeting is commonly achieved by inserting the gene of interest at or close to the locus of a cell-type-specific gene or by a strategy where the intersection of specificities, dictated by two or more genetic loci, results in cell-type targeting. The inclusion of a transgenic component in the cell-type targeting strategy excludes its use in therapy for humans, limits its range of application in preclinical, non-human primate (NHP) research and complicates its use in model organisms such as mice. The development of transgenic NHPs and mice is costly and slow, especially since cell-type targeting is often applied in the context of other genetic manipulations, such as multiple gene knockout, or when targeting different cell types with different tools.

Viral vectors for cell-type targeting may overcome such limitations. AAVs are the most frequently used vectors in both basic research and gene therapy, since they are safe for use in all tested species, including humans and NHPs, and their production is simple, cheap and fast[1]. They have three important components: the capsid for cell entry; the promoter that drives transgene expression; and the gene of interest to be expressed in the transduced cells[2,3]. Many genetic tools are small enough to fit into AAVs, different AAVs can be injected together and AAV delivery can be improved by using synthetic AAV capsids[4–6].

Potentially, cell-type targeting by AAVs could be achieved using specific promoters; however, with a few exceptions, existing promoters target expression broadly in a collection of cell types, such as inhibitory neurons, photoreceptors (PRs), retinal ganglion or bipolar cells[7–16]. It is not clear whether promoter-dependent

[1]Institute of Molecular and Clinical Ophthalmology Basel, Basel, Switzerland. [2]Friedrich Miescher Institute for Biomedical Research, Basel, Switzerland. [3]Department of Anatomy, Histology and Embryology, Semmelweis University, Budapest, Hungary. [4]Department of Ophthalmology, Semmelweis University, Budapest, Hungary. [5]Clinique vétérinaire des Halles, Strasbourg, France. [6]Faculty of Science, University of Basel, Basel, Switzerland. [7]Laboratory for Stem Cell and Retinal Regeneration, Institute of Stem Cell Research, Division of Ophthalmic Genetics, The Eye Hospital, Wenzhou Medical University, State Key Laboratory of Ophthalmology, Optometry and Visual Science, National International Joint Research Center for Regenerative Medicine and Neurogenetics, Wenzhou, China. [8]Department of Ophthalmology, University Hospital Basel, Basel, Switzerland. [9]Wilmer Eye Institute, Johns Hopkins University, Baltimore, MD, USA. [10]Present address: Epigenetics and Neurobiology Unit, European Molecular Biology Laboratory, Monterotondo, Italy. [11]Present address: Department of Laboratory Medicine, Medical School, University of Pécs, Pécs, Hungary. [12]Present address: Division of Neuroscience, San Raffaele Research Institute, Università Vita-Salute San Raffaele, Milan, Italy. [13]Present address: Genome Biology Unit, European Molecular Biology Laboratory, Heidelberg, Germany. *e-mail: jacek.krol@iob.ch; botond.roska@iob.ch

targeting can be generalized to many individual cell types. One way to search for AAVs targeting specific cell types is to screen a library of promoters driving transgene expression in brain regions of interest. An AAV promoter screen for targeting cell types has not yet been performed.

We have developed a library of 230 AAVs, each with a different synthetic promoter, most of them (226) driving an optogenetic tool fused to a fluorescent marker. First, we tested the AAVs for cell type-specific expression in the eyes of mice in vivo. Of the tested AAVs, 50% resulted in labeled retinal cells ('active AAVs') and 14% drove expression in specific cell types or cell classes ('successful targeting'). We then applied a subset of AAVs in the eyes of NHPs in vivo ($n=94$) and in human postmortem retinas in vitro ($n=84$). Of the tested AAVs, 24% led to successful targeting in NHP and 23% in human retinas. The cell types targeted by a specific synthetic promoter varied widely across mouse and primate retinas, but less so across NHP and human retinas. Then we created logic OR and AND gates using combinations of AAVs to target cell types that could not be marked by any of the AAVs alone. Finally, we show the use of cell type-specific AAVs for manipulating and recording neuronal function.

Our results demonstrate that different neuronal and glial cell types of mice, NHPs and humans can be efficiently targeted using AAVs. Furthermore, we describe a set of AAVs applicable in basic research for recording or modulating the activities of cell types, and in translational research for gene therapy of cell type-specific human diseases such as retinitis pigmentosa and macular degeneration.

Results

AAV-based cell-type targeting strategy. We created a library of 230 AAV plasmids, each equipped with a different synthetic DNA sequence with a mean length of 1249 ± 673 base pairs (bp) in the range of 113–2501 bp (Supplementary Tables 1–3) positioned 5′ of a transgene. The 5′ sequences ('synthetic promoters') were constructed using four different strategies. The synthetic promoter group ProA included sequences upstream of the start codon of selected mouse retinal cell type-specific genes[17]. Group ProB was generated by an ordered assembly of phylogenetically conserved DNA elements identified in a nucleotide sequence preceding the transcription initiation sites of a minimum of two genes with the highest cell specificity and expression indices[17]. ProC consisted of repeated transcription factor binding sites (TFBS) of cell type-specific transcription factors[17] interleaved with random sequences. ProD was identified based on an approach combining epigenome and transcriptome profiling, and consisted of low-methylated *cis*-regulatory elements transcriptionally active in different retinal cell types[18]. ProC and ProD also contained a minimal TATA box promoter element (Fig. 1a).

Of the 230 AAVs, 226 were designed to drive an optogenetic tool: a channelrhodopsin variant fused to green fluorescent protein (CatCh-GFP)[19]. The use of CatCh-GFP in the screen was based on two rationales. First, we found the expression of GFP alone to be higher than that of GFP fused to an optogenetic tool when driven by the same synthetic promoter. Since we aimed to identify synthetic promoters allowing optogenetic stimulation, we screened for the expression of CatCh-GFP. Second, the cell membrane-bound CatCh-GFP revealed the fine morphology of neuronal processes better than GFP. The remaining four AAVs were designed to express GFP.

We used three different AAV capsids appropriate for different species: AAV2/8 (ref. [20]), AAV2/9 (refs. [20,21]) and AAV2/8BP2 (ref. [9]) for adult mouse retina and AAV2/8BP2 for adult NHP and human retina (Supplementary Tables 1–3).

We developed a 'rapid AAV' protocol that increased the speed of production tenfold and used it for in vivo screens in mouse retina (Fig. 1b). The screens in NHPs and humans required substantial amounts of viral vector and were performed with AAVs produced conventionally[22].

In vivo cell-type targeting in mouse retina. We injected 920 mouse eyes subretinally with the 230 AAVs, 4 eyes for each AAV, and evaluated transgene expression 3–4 weeks later using confocal microscopy of whole-mount retinas (Fig. 1b). Of the 230 synthetic promoters tested, 113 were active (Supplementary Tables 1 and 4). Thirty-two synthetic promoters led to successful targeting, with ProDs having the highest success rate (Supplementary Tables 1 and 4). We defined targeting successful if the labeling was: (1) cell type-specific with a specificity of more than 90%; (2) cell type-specific with a specificity of more than 50% when the contamination was only Müller glia (MG, a common contamination in AAV targeting); or (3) cell class-specific with a specificity of more than 70%. To be in the successful targeting category, the expression of CatCh-GFP also had to be larger than or similar to an empirically defined threshold. Despite successful targeting by a number of AAVs, less than 1% of synthetic promoters replicated the expression specificity of their source genes. Nevertheless, synthetic promoters that targeted only outer retinal cell types were more frequently designed to target outer retinal cell types, while those that targeted only inner retinal cell types were more frequently designed to target inner retinal cell types ($P=10^{-6}$, Fisher's exact test), with only three promoters showing reverse preference (Supplementary Table 1).

Two synthetic promoters, ProA1 and ProA4, drove CatCh-GFP expression specifically in cone PRs, identified by the characteristic position of the cell bodies at the outer margin of the retinal outer nuclear layer and co-labeling with the cone-specific marker cone arrestin (CAR)[23] (Fig.1c and Supplementary Fig. 1). Nine synthetic promoters—ProA6, ProB5, ProC22, ProC32, ProD2, ProD3, ProD4, ProD5 and ProD6—were found to be rod-specific, driving CatCh-GFP expression in CAR^- outer nuclear layer cells (Fig. 1c, Supplementary Fig. 1 and Supplementary Table 1). ProC1 targeted transgene expression to both PR types (Fig. 1c).

For inner retinal neurons, we identified several synthetic promoters that labeled amacrine (AC) and ganglion cell (GC) types. These cells can be distinguished by their overall morphology and the stratification of their processes at different depths in the retinal inner plexiform layer (IPL)[24,25]. A subset of ACs (starburst ACs) with processes in two strata in the IPL were labeled with anti-choline acetyltransferase (ChAT) to provide a depth marker[26]. Two synthetic promoters, including ProC2, induced transgene expression in AII ACs and a few MG (Fig. 1c). Synthetic promoters such as ProB1 targeted other types of ACs with processes located in one stratum of the IPL (Fig. 1c). Several synthetic promoters were identified that targeted different GC types with distinguishable stratification; for example, ProD1 targeted a set of bistratified GCs with dendrites aligned with those of $ChAT^+$ ACs (Fig. 1c and Supplementary Table 1). Selective targeting of bipolar cells was rare; only AAV-ProB4 resulted in transgene expression in a type of OFF bipolar cells and cones (Supplementary Table 1). Our screen also yielded AAVs targeting non-neuronal cells. The synthetic promoters ProB2, ProA18, ProA21, ProA22 or ProD17 targeted MG, co-labeled with the specific marker cellular retinaldehyde-binding protein (CRALBP)[27] (Fig. 1c and Supplementary Table 1).

To define the cell-type targeting efficiency of selected synthetic promoters, we quantified the density of AAV-targeted $CatCh\text{-}GFP^+$ cells as a percentage of target cell type or cell class population density. AAV-ProA1 highlighted 83% of adult cones[28,29] (Fig. 1d), ProA6 targeted 50% of rods[28,29], whereas ProC1 highlighted 70% of both PRs. AAV-ProC2 targeted 34% of AII ACs expressing the specific marker Dab1 (ref. [30]), whereas ProD1 produced transgene expression in 37% of GCs with dendrites aligned with ChAT strata[31,32]. AAV-ProB2 highlighted 45% of MG expressing CRALBP[27] (Fig. 1d).

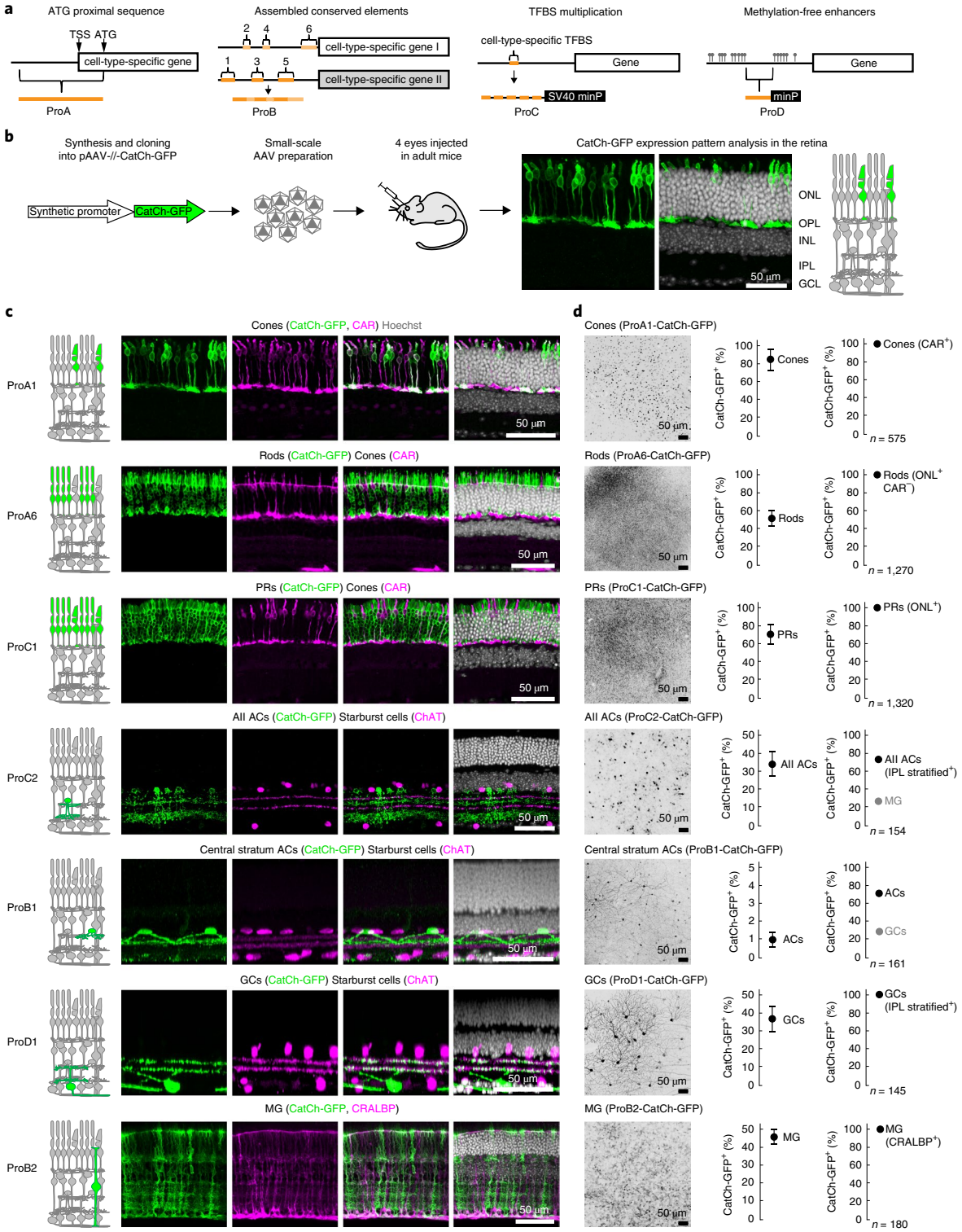

Fig. 1 | In vivo cell-type targeting in mouse retina. a, Synthetic promoter design strategies. ATG is the translation start site. **b**, Workflow for AAV-based retinal cell-type targeting screen. **c**, Confocal images of sections of AAV-infected retinas. Left: CatCh-GFP (green); middle-left, immunostaining with fluorescent marker (magenta); middle-right: CatCh-GFP and marker; right: CatCh-GFP and marker and nuclear stain (Hoechst, white). **d**, Left: confocal images of AAV-infected retinas (top view), CatCh-GFP (black). Middle: quantification of CatCh-GFP$^+$ cell density as a percentage of target cell-type or cell class density; values are the mean ± s.e.m. from $n = 12$ confocal images. Right: quantification of AAV-targeting specificity shown as a percentage of the major (black) and minor (gray) cell types or classes among cells expressing CatCh-GFP. ONL, outer nuclear layer; OPL, outer plexiform layer; INL, inner nuclear layer; GCL, ganglion cell layer.

Next, we quantified target specificity by determining the percentage of one cell type or cell class in the overall CatCh-GFP$^+$ cell population highlighted by a particular AAV. Based on morphology or marker expression, several AAVs (for example, AAV-ProA1, AAV-ProA6, AAV-ProB2, AAV-ProA4, AAV-ProD1, AAV-ProD2, AAV-ProD3, AAV-ProD4, AAV-ProD5 and AAV-ProD6) were cell

type-specific (Fig. 1d, Supplementary Fig. 1 and Supplementary Table 1). For other AAVs, target specificity was reduced by co-expression in another cell type, often MG (for example, AAV-ProC2, AAV-ProC6, AAV-ProA3). Co-labeling could potentially be eliminated using an intersectional strategy (see next section). In other cases, members of a single cell class were labeled, such as the PR cell class by AAV-ProC1 or the GC class by ProA5 (Fig.1 and Supplementary Fig. 2).

Some applications require sparse targeting of neurons of a given type, and several AAVs targeted particular cell types sparsely (Supplementary Table 1). For example, AAV-ProD2 led to expression in 2% of rods[28,29], AAV-ProC6 targeted 10% of AII ACs[30], while AAV-ProA3 infected 19% of GCs stratified in the IPL OFF-sublaminae[33] (Supplementary Fig. 1).

Taken together, screening in mouse retina identified a variety of synthetic promoters introduced into AAVs that targeted transgenes to specific mouse retinal cell types either efficiently or sparsely.

AND/OR logic for cell-type targeting. Besides AAVs targeting individual cell types, our screen also identified AAVs that targeted two or more distinct retinal cell types simultaneously (Supplementary Table 1). The overlap between cell types targeted by different AAVs provided an intersectional strategy (logic AND gate) to target a cell type, such as horizontal cells (HCs), for which no specific synthetic promoter was identified (Fig. 2a). To express CatCh-GFP in HCs, we leveraged two AAVs with ProB3 and ProC3 synthetic promoters, targeting PRs/HCs and HCs/ACs/GCs, respectively (Fig. 2b). For intersectional transgene expression, AAV-ProB3 carried a Cre-dependent double-inverted (DIO) CatCh-GFP coding sequence and AAV-ProC3 drove expression of Cre recombinase and a fluorescent mCherry marker. CatCh-GFP expression was not induced by infection of the retina with AAV-ProB3-DIO-CatCh-GFP alone. Infection solely with AAV-ProC3-Cre-mCherry produced a mixture of mCherry-labeled cell types according to ProC3 specificity. In retinas co-injected with both AAVs, CatCh-GFP was expressed only in HCs, with concomitant expression of mCherry in HCs, ACs and GCs (Fig. 2c).

Some applications require targeting of a particular combination of cell types. We tested two strategies to combine synthetic promoters to express genes in a combination of cell types targeted by individual promoters (logic OR gate; Fig. 2d). First, we fused two synthetic promoters with differing cell type specificities (Fig. 2e) within a single AAV. Eyes were injected with an AAV carrying rod-targeting ProD5 fused to bistratified GC-targeting ProD1 and driving CatCh-GFP. In all AAV-infected retinas, CatCh-GFP was expressed in bistratified GCs but not in rods, independent of the promoter structure, that is, ProD5 first or ProD1 first (Fig. 2f). The results suggested that fused sequences compromised ProD5 specificity and/or efficiency. Next, we co-injected eyes with a mixture of two different AAVs driving CatCh-GFP under ProD5 or ProD1. Dual AAV delivery efficiently targeted both rods and bistratified GCs according to promoter specificity (Fig. 2g). Thus, a combination of AAVs via AND/OR logic extends the repertoire of cell types that can be specifically targeted.

Recording and modulating activity of AAV-targeted cells. AAV-mediated cell-type targeting creates an opportunity to record or modulate the functions of specific cell types. To test whether the extent of AAV-driven transgene expression is sufficient to monitor the activity of targeted cells, we performed ex vivo and in vivo Ca^{2+} imaging during visual stimulation. In retinas infected with AAV-ProA1 expressing a fluorescent Ca^{2+} indicator (GCaMP6s) in cones (Supplementary Fig. 2), two-photon imaging revealed a strong light-evoked decrease in fluorescent traces in 93.8% of GCaMP6s-labeled cone terminals (Fig. 3a), with a polarity typical of cone physiological light responses[34]. Next, we tested light-evoked Ca^{2+} transients in MG. Glia cells sense and respond to neuronal activity through neuron-to-glia or glia-to-neuron signaling[35]. In retinas infected with AAV-ProA18, which expresses GCaMP6s in MG (Supplementary Fig. 2), two-photon imaging of cell terminals indicated a sustained increase in fluorescence in response to light (Fig. 3b) that corresponded to a light-evoked increase in Ca^{2+} (ref. [36]). The bistratified GCs targeted by AAV-ProD1 (Fig. 1c and Supplementary Fig. 2) have the typical morphology of ON-OFF direction-selective GCs. To test whether and in which direction GCs highlighted by AAV-ProD1 are tuned, we infected retinas with AAV-ProD1-GCaMP6s and analyzed cell responses following visual motion stimulation in eight different directions. Remarkably, all targeted GCs showed vertical motion selectivity, with a dominating ventrally tuned subtype (Fig. 3c). We also analyzed the visual responses of AAV-targeted cells in vivo by injecting retinas with AAV-ProA5 to introduce GCaMP6 into GCs (Supplementary Fig. 2). Neuronal activity of GCaMP6s-expressing GC axons was detected via two-photon imaging in the lateral geniculate nucleus (LGN). Light stimulation induced a substantial fluorescence increase in a subset of axonal segments (Fig. 3d). Altogether, these data demonstrate that AAV-mediated targeting allows monitoring of the activity of cells via GCaMP6s expression both ex vivo and in vivo.

We tested whether AAV-mediated cell-type targeting can modulate the activity of specific cell types. AAV-ProB4 was used to selectively target a type of retinal OFF bipolar cell, together with residual cones in *rd1* mice, a model of retinal degeneration[37] (Supplementary Fig. 2). We examined whether optical stimulation of OFF bipolar cells/cones targeted with AAV-ProB4-CatCh-GFP evokes light responses in GCs measured as spike activity using a high-density multielectrode array. CatCh-GFP activation by light stimulus led to both transient and sustained spike activity in cells in infected *rd1* retinas, but not in controls of the same age (>postnatal day 30; Fig. 3e). Thus, AAV-ProB4-induced expression of CatCh-GFP was sufficient to allow optogenetic stimulation.

To estimate the potential of each synthetic promoter to drive enough CatCh-GFP to elicit a light response, we estimated the level of GFP fluorescence driven by each promoter relative to ProB4. We defined the power of a synthetic promoter as '0' if it expressed GFP at a level similar to ProB4, '+1' if higher or '−1' if lower (Supplementary Table 1). Of the 113 synthetic promoters, 73% had a power of +1 or 0.

In vivo cell-type targeting in the NHP retina. To determine whether the generated AAVs target cell types in species other than mice, we tested their specificity in the retina of *Macaca fascicularis* (cynomolgus monkey) in vivo. We injected eyes subretinally with the 113 AAVs active in mice, administrating 4 viruses with different synthetic promoters into 4 distinct quadrants of each eye. Analysis of transgene-expressing cells 3 months postinjection identified 94 AAVs that produced reproducible expression or no expression, 62 of which were active. Twenty-three AAVs led to successful targeting (Supplementary Tables 2 and 4). PRs were targeted individually or together with other cell types by 28 AAVs (Supplementary Table 2). The 4 synthetic promoters ProA1, ProA4, ProA7 and ProB8 drove transgene expression specifically in cones, with ProA7 showing the highest targeting efficiency of 63% (ref. [38]). ProC1, ProC11 and ProD5 were rod-specific, whereas 8 others, including ProA6, targeted transgene expression to both PR types (Fig. 4, Supplementary Fig. 3 and Supplementary Table 2).

Several synthetic promoters preferentially labeled different types of ACs and GCs (Fig. 4, Supplementary Fig. 3 and Supplementary Table 2); promoters such as ProB15 and ProA5 targeted morphologically distinct GC types. Quantification of the dendritic field diameter of AAV-targeted cells showed that AAV-ProB15 targeted cells with small and compact dendritic arbors (<100 µm), whereas ProA5 highlighted GCs with larger cell bodies and dendritic fields

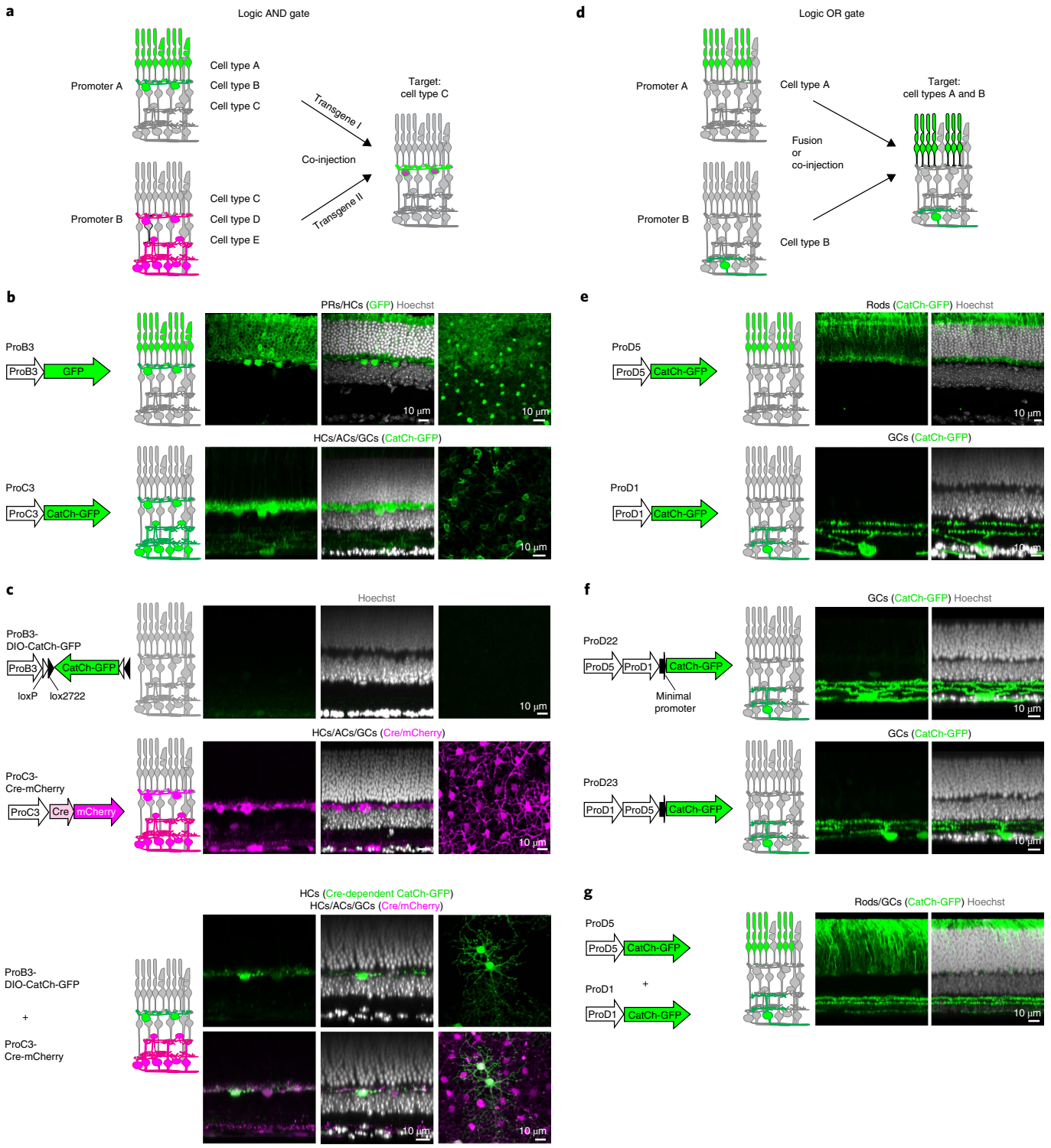

Fig. 2 | AND/OR logic for cell-type targeting by AAVs. a, Logic AND gate strategy for cell-type targeting using two AAVs that are not cell-type-specific but share one of their targets. **b**,**c**, Confocal images of AAV-infected retinas using the ProB3 or ProC3 synthetic promoters, which mutually target HCs. Left and middle: retinal section. Right: whole-mount, confocal plane at the level of HCs. The images show representative reproducible results from $n = 3$ independent experiments. **b**, AAV-ProB3-GFP (top) and AAV-ProC3-CatCh-GFP (bottom). **c**, AAV-ProB3-DIO-CatCh-GFP (top), AAV-ProC3-Cre-mCherry (middle), co-injected Cre-dependent AAV-ProB3-DIO-CatCh-GFP and AAV-ProC3-Cre-mCherry (bottom). **d**, Logic OR gate strategy for targeting selective combinations of cell types using one or more AAVs. **e**–**g**, Confocal images of AAV-infected retina sections using the ProD5 and ProD1 synthetic promoters, which target rods and bistratified GCs, respectively. Images show representative reproducible results from $n = 3$ independent experiments. **e**, AAV-ProD5-CatCh-GFP (top), AAV-ProD1-CatCh-GFP (bottom). **f**, AAV-ProD22(ProD5-ProD1)-CatCh-GFP (top), AAV-ProD23(ProD1-ProD5)-CatCh-GFP (bottom). **g**, Co-injected AAV-ProD5-CatCh-GFP and AAV-ProD1-CatCh-GFP.

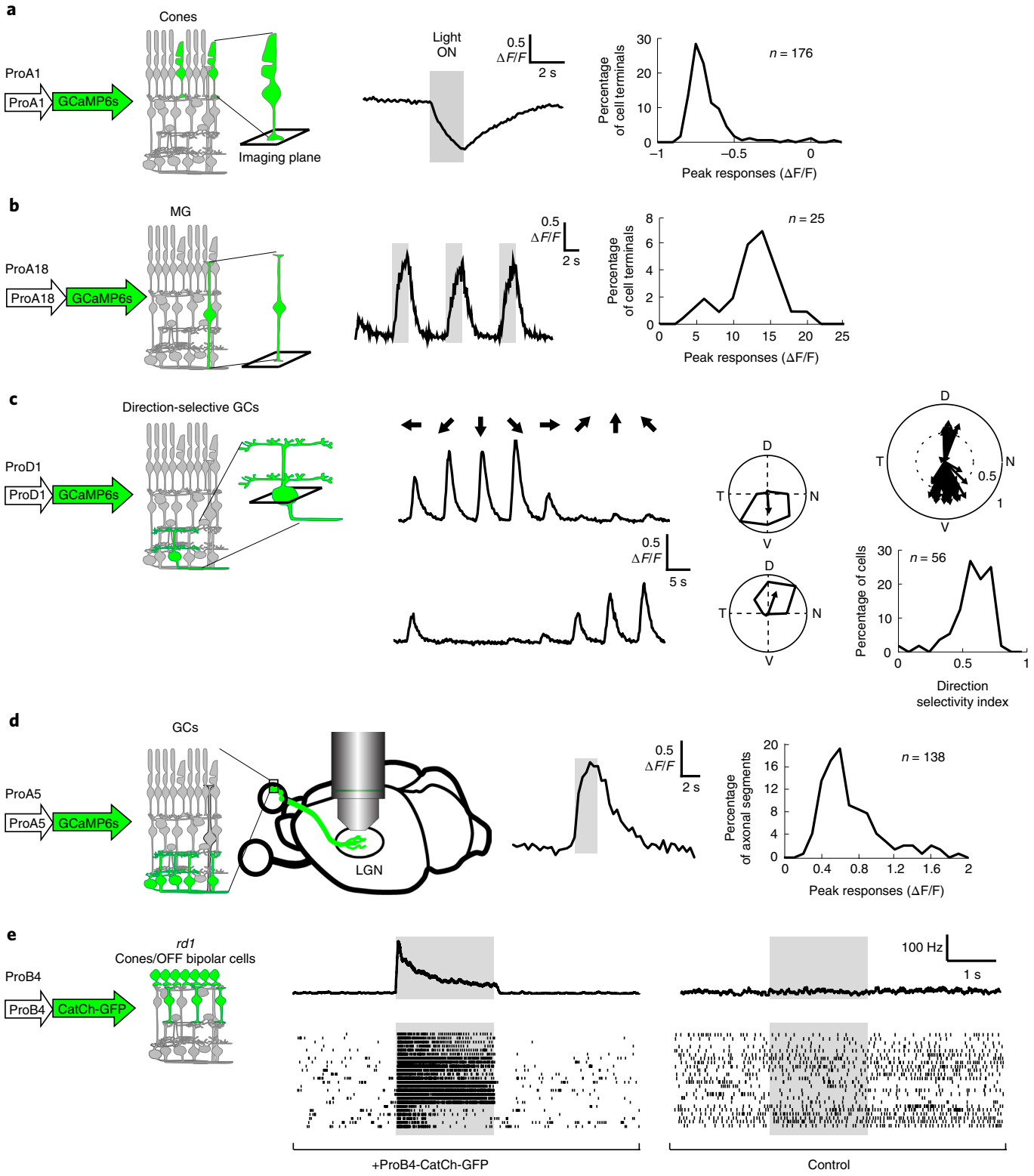

Fig. 3 | Recording and modulating activity of AAV-targeted cells. a, Left: example of light-evoked decrease in fluorescence in ProA1-targeted cone terminals expressing GCaMP6s. Right: distribution of peak responses. **b**, Left: example of light-evoked increase in fluorescence in ProA18-targeted MG terminals expressing GCaMP6s. Right: distribution of peak responses. **c**, Left: two examples (top and down) of visual motion-induced responses in ProD1-targeted GCs expressing GCaMP6s. The arrows indicate the direction of visual motion. Middle: polar plots indicate the response magnitudes of the recorded two cells normalized to the maximum response. The arrows indicate the vector sum of the responses; their direction is the preferred direction. Right: the preferred direction (arrow direction) and direction selectivity index (arrow length) of a set of GCs targeted by AAV-ProD1 (top) and the distribution of their direction selectivity index (bottom). **d**, Left: example of light-evoked increase in fluorescence in AAV-ProA5-targeted GC axon terminals in the LGN. Right: distribution of peak responses. **e**, Examples of light-evoked spike trains recorded in four GCs in *rd1* retina infected with AAV-ProB4 targeting CatCh-GFP expression to OFF bipolar cells and cones (left) and in four GCs in uninfected *rd1* retina (right). The data show reproducible results from $n = 3$ independent experiments.

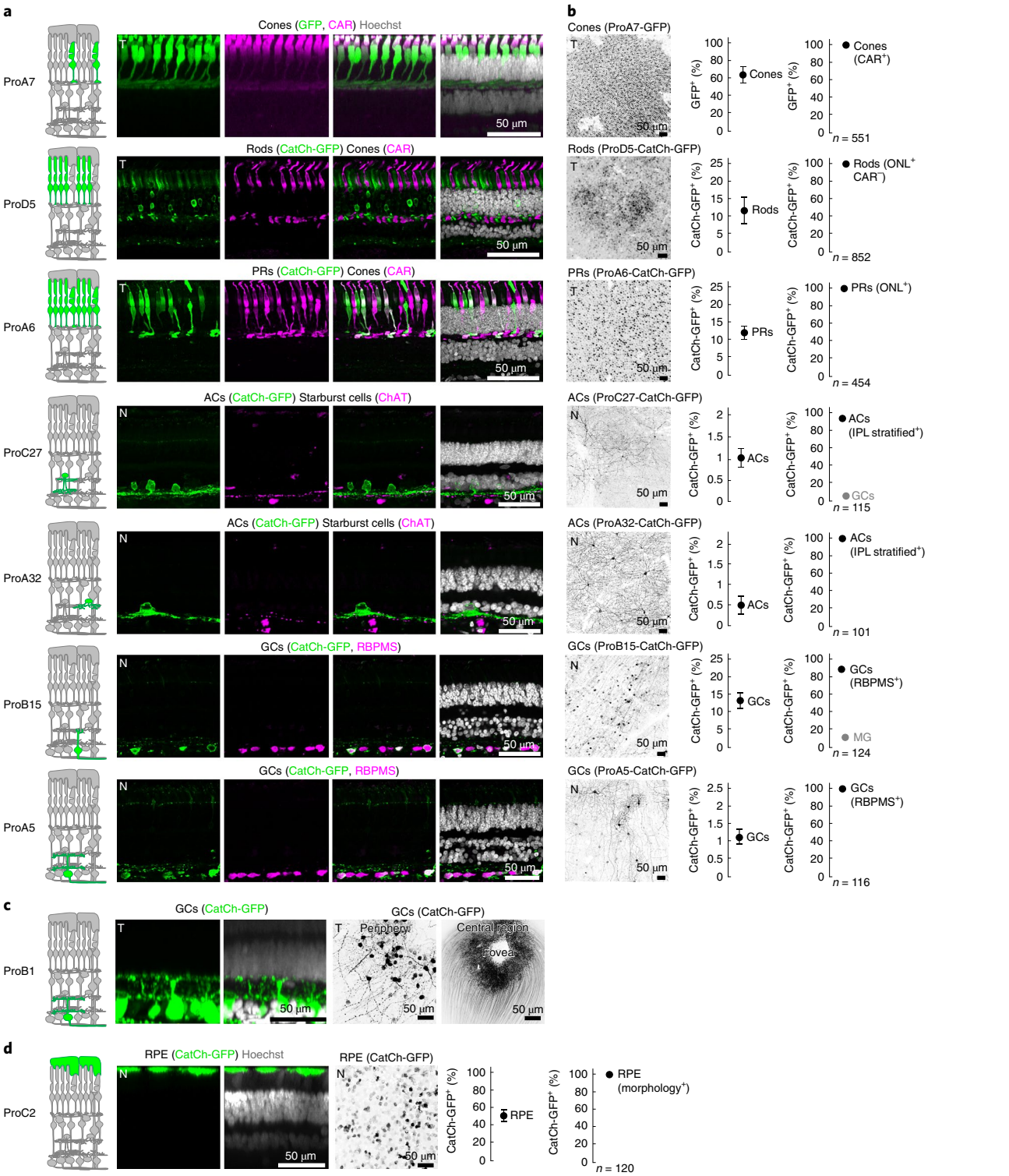

Fig. 4 | In vivo cell-type targeting in NHP retina. a, Confocal images of AAV-infected retinas. Left: GFP or CatCh-GFP (green); middle-left: immunostaining with marker (magenta); middle-right: GFP or CatCh-GFP and marker; right: GFP or CatCh-GFP and marker and nuclear stain (Hoechst, white). **b**, Left: confocal images of AAV-infected retinas (top view), GFP or CatCh-GFP (black). Middle: quantification of GFP$^+$ or CatCh-GFP$^+$ cell density as a percentage of target cell-type or cell class density; values are the mean ± s.e.m. from $n = 10$ confocal images. Right: quantification of AAV-targeting specificity shown as a percentage of the major (black) and minor (gray) cell types in cells expressing the transgene. **c**, Confocal images of AAV-ProB1-injected retina sections (left) and top views (right). Left: CatCh-GFP (green) and nuclear stain (Hoechst, white). Right: CatCh-GFP (black) in peripheral retina and around the fovea. The images show representative reproducible results from $n = 2$ independent experiments. **d**, Confocal images of a retina infected with AAV-ProC2. Left: retina sections showing CatCh-GFP (green) and nuclear stain (Hoechst, white). Middle: confocal images of AAV-infected retinas (top view), CatCh-GFP (black). Right: quantification of CatCh-GFP$^+$ cell density as a percentage of target cell-type or cell class density; values are the mean ± s.e.m. from $n = 10$ confocal images. Quantification of AAV-targeting specificity is shown as a percentage of the major (black) cell types among cells expressing the transgene. T, temporal retina quarter; N, nasal retina quarter.

(>100 µm) (Fig. 4 and Supplementary Fig. 3b). AAV-ProB1 highlighted a set of GCs with restricted stratification in two IPL strata in the peripheral retina, as well as GCs forming a circular rim around the fovea (Fig. 4c). Three synthetic promoters (ProA18, ProB4 and ProC2) drove CatCh-GFP expression exclusively in the retinal pigmented epithelium (RPE), identified by the characteristic morphology and position of CatCh-GFP$^+$ cells (Fig. 4, Supplementary Fig. 3 and Supplementary Table 2).

To test how AAV titer influences cell-type targeting, we quantified the targeting efficacy and specificity of AAV-ProA9 and AAV-ProA14 delivered at two different doses 1 log unit apart. We found no differences in targeting efficiency or specificity, suggesting that both doses were saturating (Supplementary Fig. 3c).

In vitro cell-type targeting in the human retina. Using a culture protocol we developed to keep postmortem human retinas alive for up to 14 weeks in vitro, we tested the set of 113 AAVs used in NHPs, administering them to human peripheral retina from the PR or GC side. Immunofluorescence analyses after 7 weeks identified 84 AAVs that reproducibly resulted in expression or no expression, 52 of which were active. Nineteen AAVs led to successful targeting. ProA7 preferentially targeted cones; six promoters, including ProA14, co-targeted cones and rods (Fig. 5, Supplementary Fig. 4 and Supplementary Tables 3 and 4).

The human retina contains three types of HCs that can be labeled with the marker parvalbumin[39,40]. We found that AAVs such as ProA8 sparsely targeted all three types of HCs in the adult human retina (Fig. 5 and Supplementary Table 3). Considering inner retinal neurons, we found several synthetic promoters that highlighted different types of ACs and GCs (Fig. 5). Few promoters induced CatCh-GFP expression preferentially in individual AC or GC cell types, but as many as 19 promoters co-targeted mixed cell types from both classes (Supplementary Table 3).

Finally, administration of AAV-ProC17 induced CatCh-GFP expression in MG co-labeled with CRALBP (Fig. 5).

Correlation between targeting in mouse, NHP and human retinas. For translational applications, it is useful to know whether a particular AAV targets the same cell type or class in humans as it does in mice or NHPs. Several AAVs retained their selectivity for a particular cell class across species, mostly from the ProC group (Supplementary Table 5). To quantify translatability of AAV targeting across species, we partitioned retinal cell types into eight cell groups (rods, cones, HCs, bipolar cells, ACs, GCs, MG and RPE cells). For each active AAV, we created a vector with 8 binary values; the value was 1 if expression was observed in a given cell group and 0 otherwise. We then assessed the similarity of targeting across two species in two different ways. First, by computing the Pearson correlation coefficient (R) of the vectors between the two species (Fig. 6a). Second, by computing the conditional probability of expression in a given group in one species, given expression in the same group in a second species (Fig. 6b).

The mean correlations between mice and NHPs ($R=0.339\pm0.48$) and between mice and humans ($R=0.243\pm0.44$) were significantly lower than the correlation between NHPs and humans ($R=0.60\pm0.50$, mean ± s.d.; $P=1.3\times10^{-2}$, Monte Carlo sampling of difference distribution of correlations of mice/NHPs and NHPs/humans; $P=2.4\times10^{-2}$, Monte Carlo sampling of difference distribution of correlations of mice/humans and NHPs/humans; Fig. 6a). Similarly, the conditional probability of observing expression in a cell group in NHPs or humans, given that the same AAV expresses in that group in mice, independent of the specific cell group, was significantly lower than among NHPs and humans (mice/NHPs, conditional probability = 0.377; mice/humans, conditional probability = 0.321; NHPs/humans, conditional probability = 0.667; $P=7.2\times10^{-3}$, Monte Carlo sampling of difference distribution of AAV expression in mice/NHPs and NHPs/humans; $P=1.8\times10^{-4}$, Monte Carlo sampling of difference distribution of AAV expression in mice/humans and NHPs/humans; Fig. 6b). Nevertheless, all three conditional probabilities were significantly greater than predicted from randomizing the expression pattern of each AAV across the different cell groups (mice/NHPs, $P=3.8\times10^{-8}$; mice/humans, $P=1.3\times10^{-3}$; NHPs/humans, $P=9.5\times10^{-18}$). Therefore, the ability of an AAV to target a cell group in mice is not a good predictor for targeting the same cell group in NHPs and humans, although the association is not random. On the other hand, the ability of an AAV to target a cell group in NHPs is a good predictor for targeting the same cell group in humans.

Since the expression pattern of AAV vectors in humans demonstrated a significantly greater conditional probability than expected from a randomly distributed expression pattern between mice and humans (Fig. 6b), we asked whether experiments in mice could help restrict the number of AAVs to be further tested in NHPs or humans. The conditional probabilities of an AAV expressing in a given cell group in NHPs and humans, given that it does not express in the cell group in mice, are low (mice/NHPs, conditional probability = 0.12; mice/humans, conditional probability = 0.14). Therefore, it is reasonable to eliminate AAVs for cell-type targeting in NHPs and humans based on lack of targeting in mice.

Discussion

In this study, we have described a collection of AAVs containing synthetic promoters that allow transgene expression in a broad range of retinal cell types in mice, NHPs and humans. A few AAVs containing short regulatory sequences that allowed neuronal and glial cell type or cell class targeting have been described previously[7–16]. However, there have been no reports to date of a broad spectrum of AAVs targeting neuronal or glial cell types, especially in NHPs and humans. In combination with specific AAV serotypes, we have demonstrated the use of AAV-mediated cell-type targeting for morphological characterization as well as for monitoring and modulating the activity of specific cell types.

At the core of our AAV-based, expression-targeting strategy is a synthetic promoter embedded into the AAV vector genome 5′ from the gene to be expressed. Of the four different strategies for synthetic promoter design, none yielded sequences with a dominant cell-type targeting specificity. The AAVs used in this study are episomal and do not integrate into the host cell genome (or only at a very low frequency)[41]. The molecular logic of the regulation of gene expression is probably different for episomal AAV DNA and host cell DNA.

A goal of this study was to compare targeting by AAVs across species. The probability of an AAV targeting the same cell class in mice and NHPs, or mice and humans, was as low as 0.38 and 0.32, respectively, compared with the probability for NHP and human retinal cell classes (0.67). Therefore, optimizing cell-type targeting in mice yields vectors that are unlikely to optimally target the same cell type in humans. However, our results suggest that the absence of expression in a given cell type or cell class in mice is a useful proxy for the same in humans; therefore, studies in mice can be used to eliminate AAV vectors to be tested in humans.

Our work highlighted two rules of thumb for AAV-based cell-type targeting in the retina. First, while we could not target chosen cell types, we preferentially targeted outer or inner retinal cell types when the chosen cell was in the respective group. This rule helps to restrict the choice of synthetic promoters when aiming to target a specific cell type. Second, the ProC group of promoters mostly maintained selectivity across species (Supplementary Table 5). This group of synthetic promoters could be particularly useful for translational applications.

AAVs that targeted combinations of cell types from different cell classes were not included in the successful targeting category;

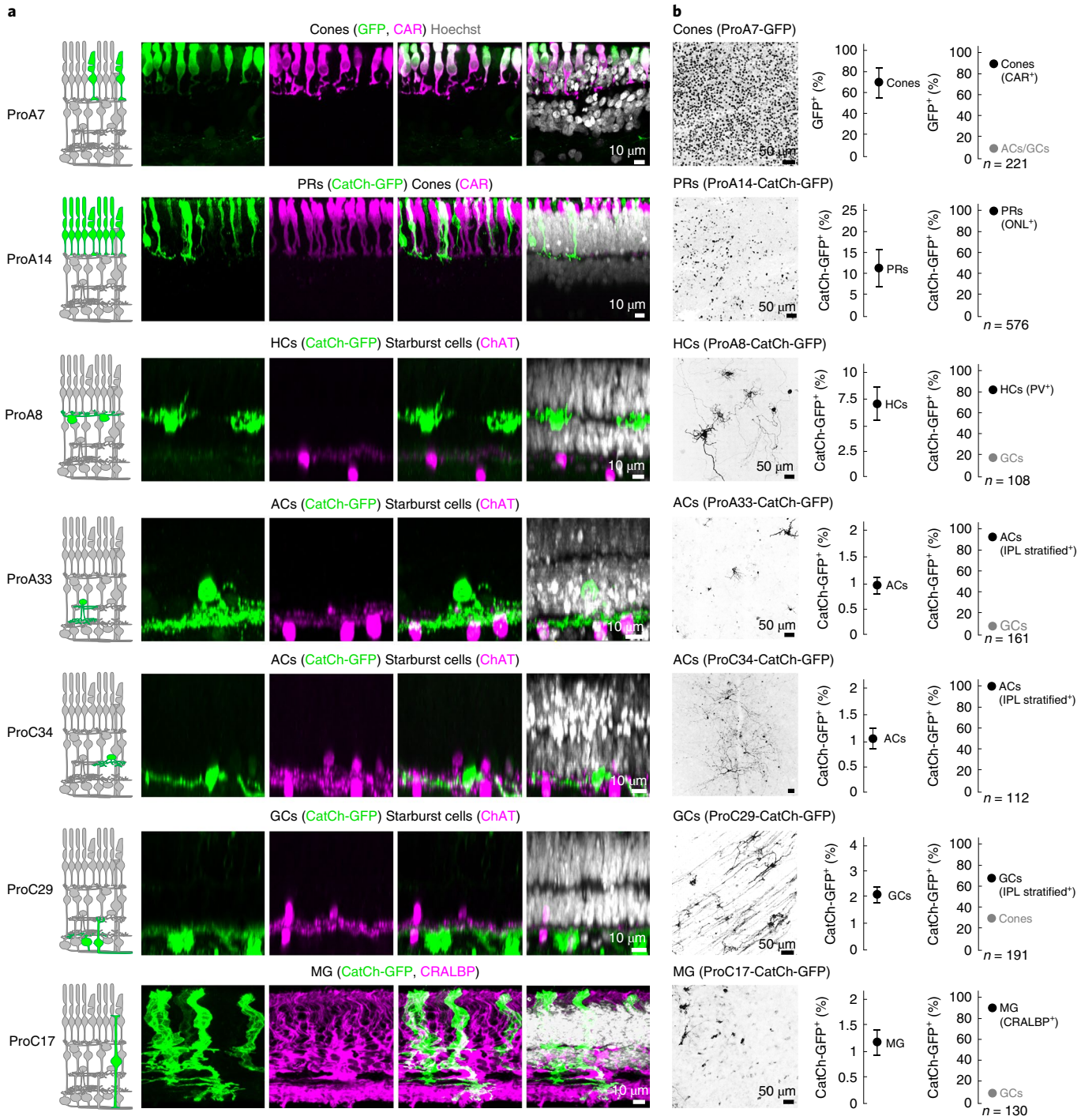

Fig. 5 | In vitro cell-type targeting in the human retina. a, Confocal images of AAV-infected retinas. Left: GFP or CatCh-GFP (green); middle-left: immunostaining with marker (magenta); middle-right: GFP or CatCh-GFP and marker; right: GFP or CatCh-GFP and marker and nuclear stain (Hoechst, white). **b**, Left: confocal images of AAV-infected retinas (top view), GFP or CatCh-GFP (black). Middle: quantification of GFP$^+$ or CatCh-GFP$^+$ cell density as a percentage of target cell-type or cell class density; values are the mean ± s.e.m. from $n = 10$ confocal images. Right: quantification of AAV targeting specificity shown as a percentage of the major (black) and minor (gray) cell types in cells expressing the transgene.

however, these AAVs could still be useful for optogenetic stimulation or for recording the visual functions of targeted cell types at single-cell resolution. We constructed an online database that includes three-dimensional confocal scans for all AAVs that yielded reproducible labeling (https://data.fmi.ch/promoterDB/). This database can be used to search for cell types labeled by active AAVs.

The AAV resources described in this study have different potentials for basic and translational research in mice, NHPs and humans.

In mice, AAVs make cell-type targeting fast and economical and can thus benefit research. First, for cell-type targeting in mutant mice, since mating mice is costly and slow. Second, when the gene of interest changes often, such as optogenetic and activity sensor genes during improvement of these tools. Third, when analyzing connectivity across different neuronal cell types, for example, by tagging one cell type with an optogenetic sensor and another with activity sensors; testing connectivity between the many possible cell type

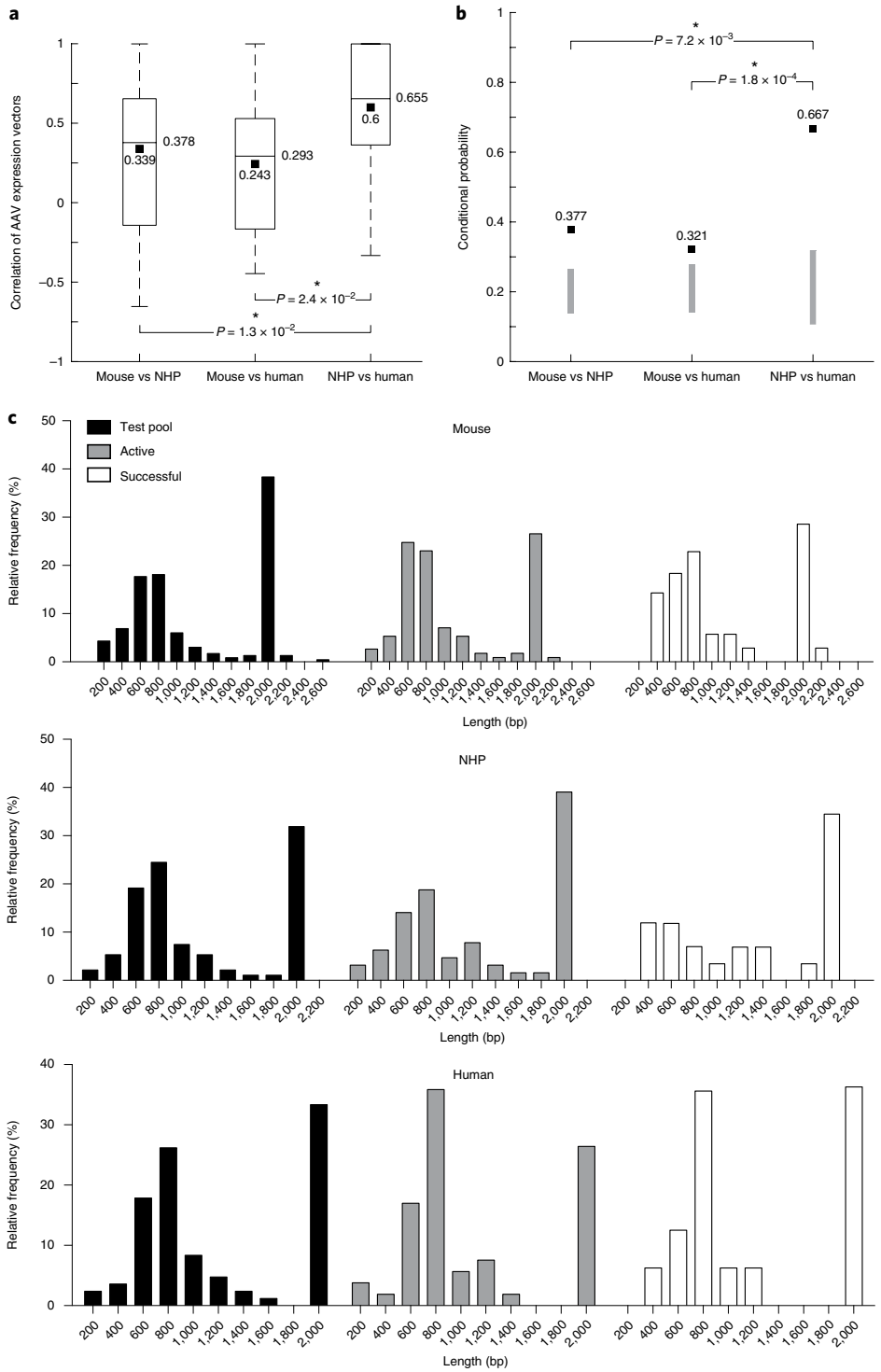

Fig. 6 | Quantitative metrics of the similarity of AAV expression in retinal cell groups in mice, NHPs and humans. a, Box-and-whisker plots (median, black line; mean, black square) showing the distribution of the correlations between the AAV expression pattern vectors in pairs of species: mouse and NHP (left; $n = 61$ biological independent samples; minimum: −0.65; 25th percentile: −0.14; median: 0.34; mean: 0.38; 75th percentile: 0.65; maximum: 1), mouse and human (middle; $n = 49$ biologically independent samples; minimum: −0.45; 25th percentile: −0.17; median: 0.24; mean: 0.30; 75th percentile: 0.53; maximum: 1) and NHP and human (right; $n = 36$ biologically independent samples; minimum: −0.33; 25th percentile: 0.36; median: 0.60; mean: 0.66; 75th percentile: 1; maximum: 1). We used Monte Carlo sampling of the difference distribution to characterize the statistical differences between the correlation of AAV expression across pairs of species; these are shown numerically (*$P < 0.05$). **b**, Mean conditional probability of AAV expression over all cell groups. Probability of expression in a cell group in one species, given expression in the same cell group in another (black squares) (solid, $P < 0.05$). The range of bars shows the distribution of conditional probabilities from a generative model of AAV expression, assuming random expression in each species (mean ± 2 s.d.; generated by randomizing the AAV expression patterns 50,000 times). Monte Carlo sampling of the difference distribution characterized the statistical difference between different conditional probabilities (*$P < 0.05$). **c**, Relative frequencies of synthetic promoters with different lengths. Test pool, all promoters tested in the retina of the indicated species; active, all promoters that led to the expression of GFP; successful, all promoters that led to successful targeting. (*$P < 0.05$).

pairs requires rapid and economic access to cell types. The ability to co-inject different AAVs to implement logic OR gates makes read/write connectivity mapping possible for cell type pairs, and possibly also for *n*-tuples of cell types. The logic AND gates can help to target cell types for which no specific promoter is available or to induce sparse labeling.

In NHPs, cell-type targeting by genome engineering is costly and time-consuming; thus, transgenic primates may be available for the study of only a few cell types. Therefore, for basic research in NHPs, AAVs offer a simple, safe and economic way to record or modulate the activity of cell types. In translational research, AAVs can be used for in vivo proof of principle for gene therapy. Since NHP genetic disease models are increasingly available, it will become possible to demonstrate proof of concept for repair in the species closest to humans. This is important, since preclinical trials in mouse models often do not translate to humans, which is consistent with our finding that retinal cell-type targeting correlates well between NHPs and humans, but much less so between mice and humans.

There is only limited knowledge about the functional roles of different cell types in the human brain. Culturing postmortem human brain parts, such as the retina or brain slices, in combination with cell-type targeting AAVs, could generate basic knowledge about, and understanding of, the organization and function of cell types in circuits in the human brain. Particularly notable for retinal research is the targeting of PRs with optogenetic tools and other cell types with genetically encoded activity sensors. Although the natural input from light is lost, restoring light sensitivity to PRs may allow computations within the human retina to be studied for several months at the level of cell types and circuits, making the human retina a simple and translationally relevant model system for research.

A prerequisite for human gene therapy is a vector system that allows efficient and long-lasting transgene expression in target cells. AAVs fulfill these criteria and are showing promise in clinical and preclinical gene therapy studies for inherited monogenic and complex eye diseases[42,43]. Gene supplementation cannot be used in the case of advanced retinal cell degeneration; therefore, alternative strategies are needed to target and modulate the remaining retinal circuitry and to restore visual functions. AAVs in our collection that target human cones (for example, ProA7) or GCs (for example, ProC29) could be used to express optogenetic tools that confer light sensitivity on remnant cells in the diseased retina[44]. For both gene supplementation and optogenetic therapy, testing cell-type targeting in human retinas in vitro significantly increases the probability that the same vector will target the desired cell type in patients in vivo. This would provide a perspective for developing effective vectors for the treatment of blindness-causing diseases such as Stargardt disease, age-related macular degeneration, Leber congenital amaurosis, retinitis pigmentosa, Leber hereditary optic neuropathy, dominant optic atrophy and glaucoma. One drawback of testing AAVs in human retinas in vitro is that not all the factors are present, such as the immune system and the influence of surrounding tissues on AAV infection. Therefore, confirmation of expression from the same vectors in NHPs is advisable before using vectors in clinical trials.

Online content

Any methods, additional references, Nature Research reporting summaries, source data, statements of code and data availability and associated accession codes are available at https://doi.org/10.1038/s41593-019-0431-2.

Received: 25 October 2018; Accepted: 17 May 2019;
Published online: 08 July 2019

References

1. Planul, A. & Dalkara, D. Vectors and gene delivery to the retina. *Annu. Rev. Vis. Sci.* **3**, 121–140 (2017).
2. Duan, D. et al. Circular intermediates of recombinant adeno-associated virus have defined structural characteristics responsible for long-term episomal persistence in muscle tissue. *J. Virol.* **72**, 8568–8577 (1998).
3. Penaud-Budloo, M. et al. Adeno-associated virus vector genomes persist as episomal chromatin in primate muscle. *J. Virol.* **82**, 7875–7885 (2008).
4. Yizhar, O., Fenno, L. E., Davidson, T. J., Mogri, M. & Deisseroth, K. Optogenetics in neural systems. *Neuron* **71**, 9–34 (2011).
5. Palfi, A. et al. Efficacy of codelivery of dual AAV2/5 vectors in the murine retina and hippocampus. *Hum. Gene Ther.* **23**, 847–858 (2012).
6. Deverman, B. E. et al. Cre-dependent selection yields AAV variants for widespread gene transfer to the adult brain. *Nat. Biotechnol.* **34**, 204–209 (2016).
7. Oh, M. S., Hong, S. J., Huh, Y. & Kim, K.-S. Expression of transgenes in midbrain dopamine neurons using the tyrosine hydroxylase promoter. *Gene Ther.* **16**, 437–440 (2009).
8. Khabou, H. et al. Noninvasive gene delivery to foveal cones for vision restoration. *JCI Insight* **3**, 96029 (2018).
9. Cronin, T. et al. Efficient transduction and optogenetic stimulation of retinal bipolar cells by a synthetic adeno-associated virus capsid and promoter. *EMBO Mol. Med.* **6**, 1175–1190 (2014).
10. Nathanson, J. L. et al. Short promoters in viral vectors drive selective expression in mammalian inhibitory neurons, but do not restrict activity to specific inhibitory cell-types. *Front. Neural Circuits* **3**, 19 (2009).
11. Dimidschstein, J. et al. A viral strategy for targeting and manipulating interneurons across vertebrate species. *Nat. Neurosci.* **19**, 1743–1749 (2016).
12. Beltran, W. A. et al. Optimization of retinal gene therapy for X-linked retinitis pigmentosa due to *RPGR* mutations. *Mol. Ther.* **25**, 1866–1880 (2017).
13. Chaffiol, A. et al. A new promoter allows optogenetic vision restoration with enhanced sensitivity in macaque retina. *Mol. Ther.* **25**, 2546–2560 (2017).
14. Hanlon, K. S. et al. A novel retinal ganglion cell promoter for utility in AAV vectors. *Front. Neurosci.* **11**, 521 (2017).
15. Dashkoff, J. et al. Tailored transgene expression to specific cell types in the central nervous system after peripheral injection with AAV9. *Mol. Ther. Methods Clin. Dev.* **3**, 16081 (2016).
16. Lu, Q. et al. AAV-mediated transduction and targeting of retinal bipolar cells with improved mGluR6 promoters in rodents and primates. *Gene Ther.* **23**, 680–689 (2016).
17. Siegert, S. et al. Transcriptional code and disease map for adult retinal cell types. *Nat. Neurosci.* **15**, 487–495 (2012).
18. Hartl, D., Krebs, A. R., Jüttner, J., Roska, B. & Schübeler, D. *Cis*-regulatory landscapes of four cell types of the retina. *Nucleic Acids Res.* **45**, 11607–11621 (2017).
19. Kleinlogel, S. et al. Ultra light-sensitive and fast neuronal activation with the Ca^{2+}-permeable channelrhodopsin CatCh. *Nat. Neurosci.* **14**, 513–518 (2011).
20. Allocca, M. et al. Novel adeno-associated virus serotypes efficiently transduce murine photoreceptors. *J. Virol.* **81**, 11372–11380 (2007).
21. Lebherz, C., Maguire, A., Tang, W., Bennett, J. & Wilson, J. M. Novel AAV serotypes for improved ocular gene transfer. *J. Gene Med.* **10**, 375–382 (2008).
22. Grieger, J. C., Choi, V. W. & Samulski, R. J. Production and characterization of adeno-associated viral vectors. *Nat. Protoc.* **1**, 1412–1428 (2006).
23. Zhu, X. et al. Mouse cone arrestin expression pattern: light induced translocation in cone photoreceptors. *Mol. Vis.* **8**, 462–471 (2002).
24. Masland, R. H. The fundamental plan of the retina. *Nat. Neurosci.* **4**, 877–886 (2001).
25. Wässle, H. Parallel processing in the mammalian retina. *Nat. Rev. Neurosci.* **5**, 747–757 (2004).
26. Haverkamp, S. & Wässle, H. Immunocytochemical analysis of the mouse retina. *J. Comp. Neurol.* **424**, 1–23 (2000).
27. Sarthy, V. P. et al. Establishment and characterization of a retinal Müller cell line. *Invest. Ophthalmol. Vis. Sci.* **39**, 212–216 (1998).
28. Jeon, C. J., Strettoi, E. & Masland, R. H. The major cell populations of the mouse retina. *J. Neurosci.* **18**, 8936–8946 (1998).
29. Ortín-Martínez, A. et al. Number and distribution of mouse retinal cone photoreceptors: differences between an albino (Swiss) and a pigmented (C57/BL6) strain. *PLoS One* **9**, e102392 (2014).
30. Rice, D. S. & Curran, T. Disabled-1 is expressed in type AII ACs in the mouse retina. *J. Comp. Neurol.* **424**, 327–338 (2000).
31. Sun, W., Li, N. & He, S. Large-scale morphological survey of mouse retinal GCs. *J. Comp. Neurol.* **451**, 115–126 (2002).
32. Salinas-Navarro, M. et al. Retinal GC population in adult albino and pigmented mice: a computerized analysis of the entire population and its spatial distribution. *Vision Res.* **49**, 637–647 (2009).
33. Kwong, J. M. K., Quan, A., Kyung, H., Piri, N. & Caprioli, J. Quantitative analysis of retinal GC survival with Rbpms immunolabeling in animal models of optic neuropathies. *Invest. Ophthalmol. Vis. Sci.* **52**, 9694–9702 (2011).
34. Yau, K.-W. & Hardie, R. C. Phototransduction motifs and variations. *Cell* **139**, 246–264 (2009).

35. Metea, M. R. & Newman, E. A. Calcium signaling in specialized glial cells. *Glia* **54**, 650–655 (2006).
36. Newman, E. A. Calcium increases in retinal glial cells evoked by light-induced neuronal activity. *J. Neurosci.* **25**, 5502–5510 (2005).
37. Farber, D. B., Flannery, J. G. & Bowes-Rickman, C. The *rd* mouse story: seventy years of research on an animal model of inherited retinal degeneration. *Prog. Retin. Eye Res.* **13**, 31–64 (1994).
38. Wikler, K. C., Williams, R. W. & Rakic, P. Photoreceptor mosaic: number and distribution of rods and cones in the rhesus monkey retina. *J. Comp. Neurol.* **297**, 499–508 (1990).
39. Kolb, H. et al. Are there three types of horizontal cell in the human retina? *J. Comp. Neurol.* **343**, 370–386 (1994).
40. Endo, T., Kobayashi, M., Kobayashi, S. & Onaya, T. Immunocytochemical and biochemical localization of parvalbumin in the retina. *Cell Tissue Res.* **243**, 213–217 (1986).
41. Smith, R. H. Adeno-associated virus integration: virus versus vector. *Gene Ther.* **15**, 817–822 (2008).
42. Weleber, R. G. et al. Results at 2 years after gene therapy for RPE65-deficient Leber congenital amaurosis and severe early-childhood-onset retinal dystrophy. *Ophthalmology* **123**, 1606–1620 (2016).
43. Russell, S. et al. Efficacy and safety of voretigene neparvovec (AAV2-hRPE65v2) in patients with RPE65-mediated inherited retinal dystrophy: a randomised, controlled, open-label, phase 3 trial. *Lancet* **390**, 849–860 (2017).
44. Roska, B. & Sahel, J.-A. Restoring vision. *Nature* **557**, 359–367 (2018).

Acknowledgements

We thank the following people: A.E. Kacso for the multielectrode array recording analyses; Z. Raics and D. Hillier for developing the recording software; N. Ledergerber for assistance in mouse breeding and maintenance; A. Drinnenberg for providing the AAV-ProA1-GCaMP6s confocal images; N. Gerber-Hollbach for help with the human eye donations; A. Police Reddy for assistance with cloning; X.W. Cheng for the eye injections; L. Vandenberghe for advice on small-scale virus preparation; D. Gaidatzis for support in ProB synthetic promoters design; T. Siegmann and R. Schmidt for creating the AAV database; C. Cepko, V. Gradinaru, E. Bamberg and K. Deisseroth for providing the plasmids; and W. Baehr for providing the anti-CAR antibody. We thank P. King, S. Oakeley and E. Macé for commenting on the manuscript. This work was supported by the Swiss National Science Foundation (grant no. CRS115_173728), the National Centre of Competence in Research (NCCR) 'Molecular Systems Engineering' (grant no. 51NF40-182895), a European Research Council Advanced Grant (funding under the European Union's Horizon 2020 research and innovation program RETMUS grant no. 669157) and a Gebert-Rüf grant (grant no. GRS-039/12) to B.R.; the NCCR 'Molecular Systems Engineering' (grant no. 51NF40-182895), the Wellcome Trust (grant no. 210572/Z/18/Z) and the Foundation Fighting Blindness Clinical Research Institute (grant no. NNCC-CL-0816-0097-UBAS-NC) to H.P.N.S.; the National Natural Science Foundation of China (grant no. 81522014), National Key Research and Development Program of China (grant no. 2017YFA0105300) and Zhejiang Provincial Natural Science Foundation of China (grant no. LQ17H120005) to Z.-B.J. We also thank Lynn and Diana Lady Dougan for a personal donation to the Institute of Molecular and Clinical Ophthalmology.

Author contributions

J.J., J.K. and B.R. designed and supervised the study. J.J., A.S., A.K., A.L., J.N., Z.Z.N., D.G. and H.P.N.S. optimized, performed and coordinated experiments on human retina culture. J.J., B.G.-S., C.P.P.-A., Ö.K. and R.I.H. performed experiments. R.K.M., S.B.R., P.H. and F.E. performed two-photon imaging or multielectrode array experiments. J.J., T.S., C.S.C., T.A., K.-C.W., R.-H.W. L.X., X.-L.F., Z.-B.J. and P.W.H. coordinated and performed experiments on NHPs. A.B. performed statistical analyses. D.H., A.R.K. and D.S. contributed to the synthetic promoter design. J.J., A.B., J.K. and B.R. wrote the paper.

Competing interest

The authors declare no competing interests.

Additional information

Supplementary information is available for this paper at https://doi.org/10.1038/s41593-019-0431-2.

Reprints and permissions information is available at www.nature.com/reprints.

Correspondence and requests for materials should be addressed to J.K. or B.R.

Peer review information: *Nature Neuroscience* thanks Liqun Luo and the other, anonymous, reviewer(s) for their contribution to the peer review of this work.

Methods

Animals, human retinal tissue and experimental models. *Mice.* Animals were used in accordance with standard ethical guidelines as stated in the European Communities Guidelines on the Care and Use of Laboratory Animals. C57BL/6J wild-type mice (6–8 weeks old) were obtained from the Charles River Laboratories. All mice were maintained in a pathogen-free environment with ad libitum access to food and drinking water. All animal experiments and procedures were approved by the Veterinary Department of the Canton of Basel-Stadt.

NHPs. Healthy cynomolgus monkeys (*Macaca fascicularis*, aged 5–19 years, weight 5.6–10.8 kg) were housed at the Kunming Biomed International, China or Simian Laboratory Europe, Strasbourg facilities. Kunming Biomed International is a facility accredited by the Association for Assessment and Accreditation of Laboratory Animal Care. Animals housed at the Simian Laboratory Europe facility were maintained and monitored in accordance with the guidelines of European Directive 2010/63/EU and handled in strict accordance with good animal practice as defined by the French National Charter on the Ethics of Animal Experimentation. All animal protocols were approved by the Institutional Animal Care and Use Committee of Kunming Biomed International or the French Ministry of Higher Education and Research (no. APAFIS#5716-2016061714424948v3).

Human retinal tissue. Human retina tissue was collected from organ donors with no reported history of eye disease at the Department of Ophthalmology at Semmelweis University, Budapest. All tissue samples were obtained in accordance with the tenets of the Declaration of Helsinki (DoH/Oct2013). Personal identifiers were removed and samples were coded before processing. All experimental protocols were approved by the local ethics committees.

Synthetic promoter design. ProA synthetic promoters were based on mouse retinal cell type transcriptome profiling[45,17,18]. The 2-kb nucleotide sequence upstream of the start codon of a highly cell type-specific gene was selected as the synthetic promoter sequence. Most of the ProA synthetic promoters contain a short (<600 bp) region corresponding to the 5′ untranslated region of the dominant transcript isoform.

To generate the ProB synthetic promoters, highly conserved sequence elements were identified by whole vertebrate genome alignments using the University of California Santa Cruz genome browser. Elements that overlapped with repeat sequences were removed and the conserved sequence elements were assigned to a gene by identifying the closest transcription start site. Conserved sequence elements far from a transcription start site were not considered or truncated in case of overlap with a transcript sequence. Conserved sequence elements were ordered according to the distance to the start codon of the closest cell type-specific gene, or randomly assembled to generate the ProB synthetic promoter sequence.

ProC synthetic promoters were based on cell type-specific TFBS[17,18] identified using the TRANSFAC (v.2013) and Jasper (v.2016) databases[46,47]. Individual ProC synthetic promoters contained the selected TFBS repeated 25 times interleaved by 15 bp random sequence spacers, followed by a TATA box containing an simian virus 40 minimal promoter (minP)[48].

ProD synthetic promoters are derived from *cis*-regulatory regions active in mouse retinal rods, cones, HCs and starburst ACs that were identified using genome-wide DNA methylation maps[18]. The sequence of interest was PCR-amplified from genomic mouse DNA (C57BL/6J) and supplemented with a synthetic minP sequence containing a TATA box (pGL4.23–28; Promega Corporation), and universal primer binding and restriction sites (5′-ATCCTCACA TGGTCCTGCTGGAGTTAGTAGAGGGTATATAATGGAAGCTCGACTTCCAG CTATCACATCCACTGTGTTGTTGTGAACTGGAATCCACTATAGGCCA).

We considered a number of factors when designing synthetic promoters. First, the mean length of our synthetic promoters was 1,249 bp. We restricted the promoters to 2.5 kb to allow insertion of a variety of transgenes. Successful targeting did not depend on promoter length in any of the species (Fig. 6c). Second, the ProC group of synthetic promoters included homo- or heterotypic clusters of TFBS, since multiplication of binding motifs has been shown to amplify transgene expression[49]. The number of TFBS was chosen to produce synthetic promoters similar in length to the other promoters. Third, we used the two different minPs to generate ProC or ProD synthetic promoters. These shared core elements, such as the TATA box and recruiting element, but differed in flanking sequences, matching the DNA synthesis/cloning strategies specific for the generation of ProC and ProD sequences.

AAV plasmid construction. Synthetic promoter sequences were chemically synthesized by GENEWIZ, with short flanks containing MluI/NheI/AscI and BamHI/EcoRI/BglII restriction sites. Synthetic promoter sequences were subcloned using an appropriate restriction site combination into pAAV-EF1a-CatCh-GFP or pAAV-hRO-GFP[50], replacing the EF1a or hRO promoters. The pAAV-EF1a-CatCh-GFP plasmid was constructed by adapter PCR and the Clontech In-Fusion kit using pcDNA3.1(-)-CatCh-GFP (a gift of E. Bamberg) and pAAV-EF1a-GFP (Roska laboratory plasmid collection). For Ca^{2+} imaging, ProA1, ProA5, ProA18 and ProD1 synthetic promoters were subcloned into pAAV-EF1a-GCaMP6s-WPRE-pGHpA via the MluI/BamHI restriction sites replacing the EF1a promoter.

To generate pAAV-ProB3-DIO-CatCh-GFP, the EF1a promoter was replaced with the ProB3 synthetic promoter using MluI/BamHI in the pAAV-EF1a-DIO-CatCh-GFP backbone (Roska laboratory plasmid collection); pAAV-ProC3-Cre/mCherry was generated using the MluI/BamHI restriction sites, replacing the EF1a promoter with ProC3 in the pAAV-EF1a-Cre/mCherry backbone (Roska laboratory plasmid collection).

AAV production and titration. HEK293T cells were co-transfected with an AAV transgene plasmid, an AAV helper plasmid encoding the AAV Rep2 and Cap proteins for the selected capsid (8, 9 or BP2), and the pHGT1-Adeno1 helper plasmid harboring the adenoviral genes (provided by C. Cepko) using branched polyethyleneimine (Polysciences). For the 'rapid AAV' protocol, one cell culture dish 15 cm in diameter was co-transfected with the plasmid mixture at 80% confluence of the HEK293T cells. A cell transfection mixture containing 7 µg AAV transgene plasmid, 7 µg Rep2 and Cap-encoding plasmid, 20 µg AAV helper plasmid and 6.8 µM polyethyleneimine in 5 ml of DMEM was incubated at room temperature for 15 min before being added to a cell culture dish containing 10 ml of DMEM. At 60 h post-transfection, cells were collected and resuspended in buffer containing 150 mM NaCl and 20 mM Tris-HCl, pH 8.0. Cells were lysed by repeated freeze–thaw cycles and $MgCl_2$ was added to make a final concentration of 1 mM. Plasmid and genomic DNA were removed by treatment with 250 U ml^{-1} of TurboNuclease at 37 °C for 10 min. Cell debris was removed by centrifugation at 4,000 r.p.m. for 30 min. AAV particles were purified and concentrated in Millipore Amicon 100 K columns (catalog no. UFC910008; Merck Millipore). Encapsidated viral DNA was quantified by TaqMan reverse transcription PCR (forward primer: GGCTGTTGGGCACTGACAA; reverse primer: CCAAGGAAAGGACGATGATTTC; probe: TCCGTGGTGTTGTCG; Thermo Fisher Scientific) following denaturation of the AAV particles using protease K; titers were calculated as genome copies per ml. For the 'conventional AAV' protocol, 10 cell culture dishes 15 cm in diameter were co-transfected with the mixture of AAV transgene, Rep2-Cap-encoding and helper plasmids at 80% confluence of the HEK293T cells. The AAVs were isolated using a discontinuous iodixanol density gradient medium (OptiPrep, catalog no. D1556; Sigma-Aldrich) and ultracentrifuged for 90 min at 242,000*g* (ref. [22]). AAV particles were purified and concentrated in Millipore Amicon 100 K columns.

AAV administration. Ocular injections were performed on mice anesthetized with 2.5% isoflurane. A small incision was made with a sharp 30-G needle in the sclera near the lens and 2 µl of AAV suspension was injected through this incision into the subretinal/intravitreal space using a blunt 5-µl Hamilton syringe (Hamilton Company) held in a micromanipulator.

For NHP ocular injections, animals were anaesthetized with ketamine (10 mg kg^{-1}; Fujian Gutian Pharmaceutical) and phenobarbital sodium (5 mg kg^{-1}; Shanghai Xinya Pharmaceutical), and were positioned facing an operating microscope (66 Vision Tech). Pupils were dilated with 0.5% tropicamide/0.5% phenylephrine hydrochloride (Santen). To visualize the fundus, a 30° circular prism (Suzhou Mingren) was placed on the surface of the cornea on top of medical sodium hyaluronate gel (Qisheng). Two 25-G pars plana sclerotomies were carried out and trocars were applied, enabling an illumination fiber (66 Vision Tech) and a 30-G needle was mounted on a 50-µl Hamilton syringe to be inserted into the vitreous chamber. Different retinal quarters were injected subretinally with 50 µl of AAV (for titer specifications, see Supplementary Table 2).

Human retinal culture. Human eyeballs were enucleated within 2 h of death under aseptic conditions and rinsed in betadine (Egis Pharmaceuticals PLC) for decontamination. The retina was dissected using fine scissors. For organotypic culture, 5 × 5 mm retinal pieces were isolated and placed GC or PR side up on polycarbonate membranes inserts (Corning). Cultures were maintained at 37 °C in 5% CO_2 in DMEM/F-12 nutrient medium (Thermo Fisher Scientific), supplemented with 0.1% BSA, 10 µM *O*-acetyl-L-carnitine hydrochloride, 1 mM fumaric acid, 0.5 mM galactose, 1 mM glucose, 0.5 mM glycine, 10 mM HEPES, 0.05 mM mannose, 13 mM sodium bicarbonate, 3 mM taurine, 0.1 mM putrescine dihydrochloride, 0.35 µM retinol, 0.3 µM retinyl acetate, 0.2 µM (±)-α-tocopherol, 0.5 mM ascorbic acid, 0.05 µM sodium selenite, 0.02 µM hydrocortisone, 0.02 µM progesterone, 1 µM insulin, 0.003 µM 3,3′,5′-triiodo-L-thyronine, 2,000 U penicillin and 2 mg streptomycin (Sigma-Aldrich). For AAV infection, 20–40 µl of individual AAV (for titer specifications, see Supplementary Table 3) was applied per retina piece. AAV-induced transgene expression was examined 6–8 weeks after virus administration.

Immunofluorescence and imaging. Retinas were fixed for 30 min in 4% (wt/vol) paraformaldehyde in PBS and washed with PBS for 24 h at 4 °C. To improve antibody penetration, retinas were subjected to freeze–thaw cycles after cryoprotection with 30% (wt/vol) sucrose. After washing in PBS, retinal whole mounts or 3% agarose-embedded (SeaKem LE Agarose; Lonza) 150-µm-thick vibratome sections (VT1000S vibratome; Leica Biosystems) were incubated for 2 h in blocking buffer containing 10% (vol/vol) normal donkey serum (Chemicon), 1% (wt/vol) BSA, 0.5% (vol/vol) Triton X-100 and 0.01% sodium azide (Sigma-Aldrich) in PBS. Primary antibody treatment was performed for 3–7 d at room

temperature in buffer containing 3% (vol/vol) NDS, 1% (wt/vol) BSA, 0.01% (wt/vol) sodium azide and 0.5% Triton X-100 in PBS. The primary antibodies used in this study were: rabbit polyclonal anti-GFP (catalog no. A-11122; RRID: AB_221569; Thermo Fisher Scientific); rat monoclonal anti-GFP (catalog no. 04404-84; RRID: AB_2313654; Nacalai); chicken polyclonal anti-GFP (catalog no. A10262; RRID: AB_2534023; Thermo Fisher Scientific); rabbit polyclonal anti-mouse CAR (catalog no. AB15282; RRID: AB_1163387; Merck Millipore); mouse monoclonal anti-primate/human CAR 7G6 (a kind gift of the W. Beahr laboratory; ref. [51]); goat polyclonal anti-ChAT (catalog no. AB144P; RRID: AB_2079751; Merck Millipore); mouse monoclonal anti-CRALBP (catalog no. RRID: AB_2269474; Abcam); rabbit polyclonal anti-red fluorescent protein (catalog no. 600-401-379; RRID: AB_2209751; Rockland); guinea pig polyclonal anti-RNA-binding protein with multiple splicing (catalog no. 1832-RBPMS; RRID: AB_2492226; PhosphoSolutions); mouse monoclonal anti-mouse parvalbumin (catalog no. MAB1572; RRID: AB_2174013; Merck Millipore); rat monoclonal anti-glycine (catalog no. IG1002; RRID: AB_10013222; ImmunoSolutions); mouse monoclonal anti-tyrosine hydroxylase (catalog no. MAB318; RRID: AB_2201528; Merck Millipore). Secondary antibody incubation was performed for 2 h at room temperature in buffer supplemented with Hoechst 33342 (10 µg ml^{-1}). The secondary antibodies used in this study were (all from Thermo Fisher Scientific unless otherwise stated): Alexa Fluor 488 donkey anti-rabbit IgG (heavy and light chains (H+L), catalog no. A-21206; RRID: AB_141708); Alexa Fluor 568 donkey anti-rabbit IgG (H+L, catalog no. A10042; RRID: AB_2534017); Alexa Fluor 647 donkey anti-rabbit IgG (H+L, catalog no. A-31573; RRID: AB_2536183); Alexa Fluor 488 donkey anti-rat IgG (H+L, catalog no. A-21208; RRID: AB_141709); Alexa Fluor 488 donkey anti-mouse IgG (H+L, catalog no. A-21202; RRID: AB_141607); Alexa Fluor 555 donkey anti-mouse IgG (H+L, catalog no. A-31570; RRID: AB_2536180); Alexa Fluor 647 donkey anti-mouse IgG (H+L, catalog no. A-31571; RRID: AB_162542); Alexa Fluor 488 donkey anti-goat IgG (H+L, catalog no. A-11055; RRID: AB_2534102); Alexa Fluor 568 donkey anti-goat IgG (H+L, catalog no. A-11057; RRID: AB_142581); Alexa Fluor 633 donkey anti-goat IgG (H+L, catalog no. A-21082; RRID: AB_141493); Cy3-AffiniPure donkey anti-rat IgG (H+L, catalog no. 12-165-153; RRID: AB_2340667; Jackson ImmunoResearch Laboratories); Alexa Fluor 488-conjugated donkey anti-chicken IgY (catalog no. 703-545-155; RRID:AB_2340375; Jackson ImmunoResearch Laboratories); donkey anti-guinea pig Cy3-AffiniPure (catalog no. 706-165-148; RRID: AB_2340460; Jackson ImmunoResearch Laboratories). After washing in PBS, retinas were embedded in ProLong Gold Antifade Mountant (Thermo Fisher Scientific).

An LSM 700 laser scanning confocal microscope (Zeiss) was used to acquire images of antibody-stained retinas with an EC Plan-Neofluar 40×/1.30 oil M27 objective and a Plan-Acro Achromat 10×/0.45 objective at up to four excitation laser lines according to secondary antibody specification. Cell-type morphologies were assessed from 512 × 512 pixel images in a *z*-stack with 0.85 µm *z*-steps. Images were processed using the Imaris software (v.9.0.2, Bitplane). Data collection and analysis were not blind to the conditions of the experiments.

Two-photon calcium imaging in the retina. Retinas infected with AAV-ProA1-GCaMP6s, AAV-ProA18-GCaMP6s and AAV-ProD1-GCaMP6s were isolated and the pigment epithelium was removed in Ringer's solution (110 mM NaCl, 2.5 mM KCl, 1 mM $CaCl_2$, 1.6 mM $MgCl_2$, 10 mM D-glucose, 22 mM $NaHCO_3$, bubbled with 5% CO_2/95% O_2, pH 7.4) and mounted GC side up on a filter microfiltration membrane (Merck Millipore) with a 2-mm rectangular aperture in the center. Retinas were superfused in Ringer's solution at 35–36 °C in the microscope chamber for the duration of the experiment. The two-photon microscope system has been described previously[52]. Briefly, the system was equipped with a Mai Tai HP two-photon laser tuned to 920 nm (Spectra-Physics) and a 60× objective (Fluor, 1.0 numerical aperture; Nikon). Image data were acquired using custom software developed by Z. Raics (SELS Software), taking images of 150 × 150 pixels (10 frames s^{-1} for ProA1 and ProA18) or 200 × 200 pixels (5.7 frames s^{-1} for ProD1). A Transistor-Transistor Logic signal generated at the end of each line scan of the horizontal scanning mirror was used to trigger an ultraviolet LED projector (Acer)[53]. To prevent the stimulation light bleeding through and masking light emission from the sample, stimuli were presented exclusively during the fly-back period of the horizontal scanning mirror. Visual stimulation was generated via custom-made software (Python, LabVIEW; National Instruments). The light intensity of the visual stimulation was 7.2×10^4 photoisomerizations per rod per s (R* s^{-1}) with a background intensity of 1.4×10^2 R* s^{-1}. For AAV-ProA1 and ProA18, the stimulation was a flash of a circular light spot 120 µm in diameter presented for 2 s. For AAV-ProD1, the stimuli were circular light spots of 400 µm moving at a speed of 800 µm s^{-1} on the retina in 8 different directions.

Fluorescence data were analyzed semi-online via custom-made software written in Python by Z. Raics. For ProA1, the cone axon terminals were automatically segmented via an algorithm developed by D. Hillier[54]. For ProA18 and ProD1, the terminal areas and the cell bodies were segmented manually. Background fluorescence was calculated as the mean of the 10% dimmest pixels for each frame and subtracted from the mean fluorescence of each segmented area. The resulting fluorescence values were then normalized as ΔF/F, where F represents baseline (mean fluorescence of a 1–2 s time window before the onset of the stimulus). In the case of repetitive stimulation, all responses to different trials were averaged before calculating the peak response. Peak responses (ProA1 and ProA18) and preferred direction and direction-selective index (ProD1) were analyzed offline using MATLAB (R2016a and R2018a, MathWorks). The peak responses in the cone axon terminals (ProA1) were calculated as the means of ΔF/F values during the second half of the stimulation period. Peak responses in MG (ProA18) were the point of maximum fluorescence in the stimulation period. The preferred direction and direction-selective index (ProD1) were calculated as described previously[55]. Briefly, for the cell of interest, eight vectors were formed first, each associated with motion along a different direction. The angle of the vector was the angle corresponding to the motion direction (0°, 45°, 90°, 135°, 180°, 225°, 270°, 315°). The length of each vector was the response amplitude along the relevant direction, where the amplitude was defined as the maximum ΔF/F in the peak. The preferred direction and direction-selective index of the cell of interest were calculated as the angle and length of the sum of the eight vectors divided by the sum of the lengths of the eight vectors, respectively. Cells that showed no significant responses (signal-to-noise-ratio < 50, where signal-to-noise-ratio is defined as the amplitude of the largest peak divided by the s.d. of the baseline) were excluded from the analysis. Finally, response histograms were assembled and plotted.

Two-photon imaging of GC axons in the LGN. AAV-ProA5-GCaMP6s was administered into the right mouse retina as described earlier. After 3–4 weeks, mice were anesthetized with fentanyl/medetomidine/midazolam (fentanyl 0.05 mg kg^{-1}, medetomidine 0.5 mg kg^{-1}, midazolam 5.0 mg kg^{-1}) and placed in a stereotaxic frame (SR-5M-HT; Narishige). Liquifilm (Allergan) was applied to the eyes to prevent dehydration during surgery. A metal bar for head fixation during imaging was glued to the skull[56]. A 3-mm diameter craniotomy was made above the LGN. The exposed cortex and the underlying hippocampus were aspirated, exposing the LGN. The tissue was kept moist with mouse Ringer's solution (135 mM NaCl, 5.4 mM KCl, 5 mM HEPES, 1.8 mM $CaCl_2$, pH 7.2) heated to 37 °C. A 2-mm diameter glass coverslip was slightly pushed against the LGN, while the tissue between the edges of the coverslip and the skull were covered with superglue and allowed to solidify. After surgery, the anesthetized mice were placed under a two-photon microscope. Retinal GC axons in the left LGN were imaged through a 40× objective (LUMPlanFl 40×/0.8 numerical aperture water immersion objective; Olympus) between 20 and 50 µm from the surface of the LGN. Each mouse was presented with six flashes of blue light, each lasting 5 s, with 10 s between each light flash. Blue light was produced by a mounted light-emitting diode (part no. M405L3; Thorlabs) focused with an achromatic doublet lens (part no. AC254–030-A-ML; Thorlabs) onto a fiber-optic cable (part no. M58L005; Thorlabs), which was placed in front of the mouse to project full-field light onto the right eye. GCaMP6s responses were collected at 3 Hz (LabVIEW v.2012; National Instruments) and analyzed in MATLAB (R2016a and R2018a, MathWorks). Each retinal GC axon segment was selected manually and ΔF/F was calculated by dividing the average pixel intensity within the region of interest for each time point by the mean signal intensity for that region of interest during the 5 s before visual stimulation. An average light response trace was obtained by averaging the responses over the six light flashes. Peak responses were calculated from the maximal ΔF/F of the average light responses in each axon segment during the 5 s of light stimulation.

Multielectrode array recordings. To record the spike trains of retinal GCs, the retina of a wild-type C57BL/6J mouse or a mutant *rd1* mouse infected with AAV-ProB4-CatCh-GFP was isolated under dim red light in Ringer's solution (110 mM NaCl, 2.5 mM KCl, 1 mM CaCl2, 1.6 mM $MgCl_2$, 10 mM D-glucose, 22 mM $NaHCO_3$) bubbled with 5% CO_2/95% O_2. The retina, GC side down, was then immobilized on the multielectrode array by gently pressing with a cell culture membrane (Transwell, catalog no. 3450r; Corning) bearing hexagonally arranged holes of 200 µm diameter and a center-to-center distance of 400 µm. For the duration of the experiment, the retina was perfused with oxygenated Ringer's solution (110 mM NaCl, 2.5 mM KCl, 1.0 mM $CaCl_2$, 1.6 mM $MgCl_2$, 22 mM $NaHCO_3$, 10 mM D-glucose, pH 7.4, with 5% CO_2/95% O_2) at a flow rate of 1.5 ml min^{-1} at 35 °C. Extracellular voltage was measured with a multielectrode array (MEA1060 Up-BC amplifier; Multichannel Systems) at 20 kHz. The array was fixed onto a motorized table (Scientifica). CatCh was activated by a light stimulus (7×10^{16} photons cm^{-2} s^{-1}) generated using a digital light processing projector (PLUS U137SF; KAGA) and projected onto the retina by the condenser lens of an inverted microscope (Nikon TE300). The spectrum of the stimulus light was determined using a spectrophotometer (Ocean Optics USB2000; Ocean Optics) and the light intensity was measured using a power meter (part no. S130VC; Thorlabs). The stimulation intensity was calculated by integrating the product of the projector spectrum and the normalized absorption spectrum of CatCh-GFP. The recorded voltage was bandpass-filtered (400–4000 Hz) and spikes were sorted using the UltraMegaSort2000 software (v.2012; Kleinfeld Laboratory, University of California San Diego). The spike frequency was calculated using 50-ms moving bins. Intrinsically photosensitive retinal GCs were discriminated by their delayed spiking. For quantification, only spike frequency values in the first 200 ms after light start or end were used.

Definitions, quantification and statistical analysis. *Target density.* Target density was defined as the percentage density of labeled cells of the most abundant type or class relative to the total density of the target cell type or class. Published mean densities (cells mm^{-2}) were used as a reference. Mice: CAR$^+$ cones[23,28,29]; rods[28,29]; HCs[28]; OFF bipolar cells[57]; MG[28]; Dab1$^+$ aII ACs[30]; INL ACs[58]; bistratified GCs[31,32]; RBPS$^+$ GCs[33]; and OFF-sublaminae stratified GCs[28,33]. NHPs: retinal pigmented epithelial cells[59]; PRs[38], INL ACs[60]; and mid-periphery GCs[61,62]. Humans: PRs[63]; parvalbumin$^+$ HCs[39,40]; MG[64]; ACs[65–67]; and GCs[65].

Target specificity. Target specificity was defined as the percentage of labeled cells of a given type or class relative to all labeled cells.

Working definition of a cell type. We defined a collection of retinal cells a cell type if the collection was labeled by a marker of a previously characterized retinal cell type, if the morphologies of the cells had the same unique characteristic of a known cell type or if the axons or dendrites of labeled cells were restricted to the same layer in the IPL.

Successful targeting. We defined successful targeting if the labeling was (1) cell type-specific with a specificity of more than 90%, (2) cell type-specific with a specificity of more than 50% when the contamination consisted of only MG (a common contamination in AAV targeting) or (3) cell class-specific with specificity of more than 70%. In each category, the target density had to be larger than 0.5% and the expression of CatCh-GFP had to be larger or similar to an empirically defined threshold determined by the expression of CatCh-GFP in the mouse retina driven by the ProB4 synthetic promoter, which drove enough CatCh-GFP to elicit light responses from the targeted cells.

Reproducibility. Results are only reported for synthetic promoters that passed a reproducibility criterium. The reproducibility criterium in mice for active promoters was that the dominant labeled cell type was the same in at least three out of four eye injections. The criterium for inactive promoters was the absence of labeling in at least three out of four eye injections. Accordingly, all 230 synthetic promoters passed the reproducibility criterium. In NHPs, promoters were defined reproducible when the dominant labeled cell type was the same in two out of two injections. For inactive promoters, no labeling was observed in two out of two injections. Out of 113 synthetic promoters tested, 94 were reproducible. Application of the same criterium to humans resulted in 84 out of 113 synthetic promoters that were reproducible.

Sample sizes were not predetermined statistically but were based on the size of the AAV test pool, availability, reproducibility criteria (see Definitions, quantification and statistical analysis), animal experimentation permits and the availability of human retinal donations. Animals were allocated randomly into experimental groups independent of sex and age. Human retina donations were anonymized.

Correlation. The expression pattern of each AAV was divided into eight cell classes: rods; cones; HCs; bipolar cells; ACs; GCs; MG; and RPE cells. Ignoring the relative penetrance of each AAV, the expression in each class was binarized. We computed the Pearson correlation coefficient of the expression vector in each pair of species for every AAV tested in both species. The reported results are the first-order statistics (mean, median; s.d., median) over the set of correlations for all AAVs in each pair of species. The correlation is a metric ranging in value from −1 to 1; if both expression pattern vectors are identical, the correlation is 1; if the expression in both species in every cell class is different, the correlation is −1.

Monte Carlo sampling of difference distribution of correlations. We computed the statistical significance of the difference in the mean Pearson correlation coefficient between two different pairs of species, by using the two vectors of the underlying correlations (each composed of the Pearson correlation coefficients of all the AAVs tested in each pair of species). We concatenated both vectors and resampled two new vectors (of the same size as each original vector). We generated a new random variable that was the difference between the mean of these two new vectors, sampling from a new distribution, which we termed the 'difference distribution'. Given the null hypothesis that the two distributions are statistically identical, this random variable will be normally distributed around 0. We repeatedly sampled from the difference distribution, computing all possible samples (up to a maximum of 50,000) and then computed the mean and standard deviation of the distribution. The true difference between the mean correlations between two pairs of species can be viewed as a potential sample from the difference distribution. Computing its z-score relative to the distribution then allowed us to compute the bounding probability that it is actually a sample from the difference distribution, which we have reported in the text.

Conditional probability. As before, the expression pattern of each AAV was divided into eight retinal cell classes and appropriately binarized. For each pair of species, we counted the number of instances where an AAV was expressed in the same cell class in both species, independent of cell class. We then normalized this by the total number of times an AAV was expressed in each cell class in the first species (for example, expression in the mouse in the mouse/human pair), again independent of cell class. This gives an estimate of the probability that an AAV will be expressed in a cell class, given that it is expressed in the same cell class in one species, independent of the specific cell class. For the conditional probability given the lack of expression, we followed an analogous process.

Monte Carlo sampling of difference distribution of AAV expression. We have reported two statistical tests of significance for the conditional probability: (1) the probability that the observed conditional probability of expression was actually drawn, in each species, independently from a random distribution. We generated this artificial distribution by randomly permuting the cell class where each AAV was expressed, controlling for the number of cell classes where it was expressed. We then generated 50,000 such randomized samples of AAV expression in each of the two species. For each example, we computed the mean conditional probability between the two species, generating a sample from the distribution of conditional probability assuming that the expression of each AAV is independent between species. Since this distribution may not be normal, we computed the significance as introduced in the previous section, through the use of a difference distribution. In this case, the two vectors are of unequal size: the first contains the single observed value and the second contains the 50,000 samples from the distribution derived from randomizing AAV expression. Computing the z-score of the difference between the observed value and the sampled distribution provided us with the probability that the observed conditional probability is actually sampled from a random distribution, which we have reported; (2) the probability that the observed conditional probability of expression in one pair of species is significantly different from the same in a second pair of species. Again, making no assumption about the underlying distribution, we used the same approach of generating a difference distribution. For each pair of species, we generated a vector of the conditional probability by normalizing the number of cell classes where an AAV was expressed in the same cell class in both species by the total number of cell classes where the AAV was expressed in the first species. Then, using these two conditional probability vectors, we computed the difference distribution. As before, we sampled the difference distribution and use the z-score of the observed difference in conditional probability between the two pairs of species to compute the bounding probability that the two observed samples are actually from the same underlying distribution.

Reporting Summary. Further information on research design is available in the Nature Research Reporting Summary linked to this article.

Data availability

The AAV expression patterns of synthetic promoters described here have been made available in a public database (https://data.fmi.ch/promoterDB/). Further information and requests for resources and reagents should be directed to and will be fulfilled by the lead contact, B. Roska (botond.roska@iob.ch) on signing a material transfer agreement.

Code availability

The computer codes and algorithms used in this study are available upon reasonable request.

References

45. Siegert, S. et al. Genetic address book for retinal cell types. *Nat. Neurosci.* **12**, 1197–1204 (2009).
46. Matys, V. et al. TRANSFAC: transcriptional regulation, from patterns to profiles. *Nucleic Acids Res.* **31**, 374–378 (2003).
47. Mathelier, A. et al. JASPAR 2016: a major expansion and update of the open-access database of transcription factor binding profiles. *Nucleic Acids Res.* **44**, D110–D115 (2016).
48. Byrne, B. J., Davis, M. S., Yamaguchi, J., Bergsma, D. J. & Subramanian, K. N. Definition of the simian virus 40 early promoter region and demonstration of a host range bias in the enhancement effect of the simian virus 40 72-base-pair repeat. *Proc. Natl Acad. Sci. USA* **80**, 721–725 (1983).
49. Smith, R. P. et al. Massively parallel decoding of mammalian regulatory sequences supports a flexible organizational model. *Nat. Genet.* **45**, 1021–1028 (2013).
50. Busskamp, V. et al. Genetic reactivation of cone photoreceptors restores visual responses in retinitis pigmentosa. *Science* **329**, 413–417 (2010).
51. Zhang, H. et al. Identification and light-dependent translocation of a cone-specific antigen, cone arrestin, recognized by monoclonal antibody 7G6. *Invest. Ophthalmol. Vis. Sci.* **44**, 2858–2867 (2003).
52. Yonehara, K. et al. The first stage of cardinal direction selectivity is localized to the dendrites of retinal GCs. *Neuron* **79**, 1078–1085 (2013).
53. Reiff, D. F., Plett, J., Mank, M., Griesbeck, O. & Borst, A. Visualizing retinotopic half-wave rectified input to the motion detection circuitry of *Drosophila*. *Nat. Neurosci.* **13**, 973–978 (2010).
54. Drinnenberg, A. et al. How diverse retinal functions arise from feedback at the first visual synapse. *Neuron* **99**, 117–134.e11 (2018).

55. Wertz, A. et al. Single-cell-initiated monosynaptic tracing reveals layer-specific cortical network modules. *Science* **349**, 70–74 (2015).
56. Holtmaat, A. et al. Long-term, high-resolution imaging in the mouse neocortex through a chronic cranial window. *Nat. Protoc.* **4**, 1128–1144 (2009).
57. Strettoi, E., Novelli, E., Mazzoni, F., Barone, I. & Damiani, D. Complexity of retinal cone bipolar cells. *Prog. Retin. Eye Res.* **29**, 272–283 (2010).
58. Pérez de Sevilla Müller, L., Azar, S. S., de Los Santos, J. & Brecha, N. C. Prox1 is a marker for aII amacrine cells in the mouse retina. *Front. Neuroanat.* **11**, 39 (2017).
59. Snodderly, D. M., Sandstrom, M. M., Leung, I. Y.-F., Zucker, C. L. & Neuringer, M. Retinal pigment epithelial cell distribution in central retina of rhesus monkeys. *Invest. Ophthalmol. Vis. Sci.* **43**, 2815–2818 (2002).
60. Martin, P. R. & Grünert, U. Spatial density and immunoreactivity of bipolar cells in the macaque monkey retina. *J. Comp. Neurol.* **323**, 269–287 (1992).
61. Wässle, H., Grünert, U., Röhrenbeck, J. & Boycott, B. B. Retinal GC density and cortical magnification factor in the primate. *Vision Res.* **30**, 1897–1911 (1990).
62. Kim, C. B. Y., Tom, B. W. & Spear, P. D. Effects of aging on the densities, numbers, and sizes of retinal GCs in rhesus monkey. *Neurobiol. Aging* **17**, 431–438 (1996).
63. Jonas, J. B., Schneider, U. & Naumann, G. O. Count and density of human retinal photoreceptors. *Graefes Arch. Clin. Exp. Ophthalmol.* **230**, 505–510 (1992).
64. Dreher, Z., Robinson, S. R. & Distler, C. Müller cells in vascular and avascular retinae: a survey of seven mammals. *J. Comp. Neurol.* **323**, 59–80 (1992).
65. Curcio, C. A. & Allen, K. A. Topography of GCs in human retina. *J. Comp. Neurol.* **300**, 5–25 (1990).
66. Kolb, H., Linberg, K. A. & Fisher, S. K. Neurons of the human retina: a Golgi study. *J. Comp. Neurol.* **318**, 147–187 (1992).
67. MacNeil, M. A., Heussy, J. K., Dacheux, R. F., Raviola, E. & Masland, R. H. The shapes and numbers of ACs: matching of photofilled with Golgi-stained cells in the rabbit retina and comparison with other mammalian species. *J. Comp. Neurol.* **413**, 305–326 (1999).

nature research

Corresponding author(s): Botond Roska

Last updated by author(s): May 10, 2019

Reporting Summary

Nature Research wishes to improve the reproducibility of the work that we publish. This form provides structure for consistency and transparency in reporting. For further information on Nature Research policies, see Authors & Referees and the Editorial Policy Checklist.

Statistics

For all statistical analyses, confirm that the following items are present in the figure legend, table legend, main text, or Methods section.

n/a	Confirmed	
☐	☒	The exact sample size (*n*) for each experimental group/condition, given as a discrete number and unit of measurement
☐	☒	A statement on whether measurements were taken from distinct samples or whether the same sample was measured repeatedly
☐	☒	The statistical test(s) used AND whether they are one- or two-sided *Only common tests should be described solely by name; describe more complex techniques in the Methods section.*
☐	☒	A description of all covariates tested
☐	☒	A description of any assumptions or corrections, such as tests of normality and adjustment for multiple comparisons
☐	☒	A full description of the statistical parameters including central tendency (e.g. means) or other basic estimates (e.g. regression coefficient) AND variation (e.g. standard deviation) or associated estimates of uncertainty (e.g. confidence intervals)
☐	☒	For null hypothesis testing, the test statistic (e.g. *F*, *t*, *r*) with confidence intervals, effect sizes, degrees of freedom and *P* value noted *Give P values as exact values whenever suitable.*
☒	☐	For Bayesian analysis, information on the choice of priors and Markov chain Monte Carlo settings
☒	☐	For hierarchical and complex designs, identification of the appropriate level for tests and full reporting of outcomes
☐	☒	Estimates of effect sizes (e.g. Cohen's *d*, Pearson's *r*), indicating how they were calculated

Our web collection on statistics for biologists contains articles on many of the points above.

Software and code

Policy information about availability of computer code

Data collection	custom software developed by Z. Raics (SELS Software, Hungary), custom made software (Python, Labview, National Instruments) for visual stimulation
Data analysis	custom-made software written in Python by Z. Raics (SELS Software, Hungary), UltraMegaSort software (Kleinfeld Lab, University of California, San Diego)

For manuscripts utilizing custom algorithms or software that are central to the research but not yet described in published literature, software must be made available to editors/reviewers. We strongly encourage code deposition in a community repository (e.g. GitHub). See the Nature Research guidelines for submitting code & software for further information.

Data

Policy information about availability of data

All manuscripts must include a data availability statement. This statement should provide the following information, where applicable:

- Accession codes, unique identifiers, or web links for publicly available datasets
- A list of figures that have associated raw data
- A description of any restrictions on data availability

The AAV expression pattern of synthetic promoters described here have been made available in a public database (https://data.fmi.ch/promoterDB/)

Field-specific reporting

Please select the one below that is the best fit for your research. If you are not sure, read the appropriate sections before making your selection.

☒ Life sciences ☐ Behavioural & social sciences ☐ Ecological, evolutionary & environmental sciences

Life sciences study design

All studies must disclose on these points even when the disclosure is negative.

Sample size	No statistical method was used to pre-determine sample sizes. Sample sizes were defined based to AAV test pool size, availability, reproducibility criterium (see below), animal experimentation permits, and the availability of human retinal donations.
Data exclusions	Data was excluded if it did not pass reproducibility criteria (see below)
Replication	The reproducibility criterium in mice for active promoters was that the dominant labeled cell type was the same in at least three out of four eye injections. The criterium for inactive promoters was the absence of labeling in at least three out of four eye injections. Accordingly, all 230 synthetic promoters passed the reproducibility criterium. In non-human primates, promoters were defined reproducible when the dominant labeled cell type was the same in two out of two injections. For inactive promoters, no labeling was observed in two out of two injections. Out of 113 synthetic promoters tested, 94 were reproducible. Application of the same criterium to humans resulted in 84 out of 113 synthetic promoters reproducible.
Randomization	Animals were allocated randomly into experimental groups regarding sex and age. Human retina donations were anonymized.
Blinding	Investigators were not blinded during data collection and analysis because knowledge of experimental conditions was required during data collection and evaluation.

Reporting for specific materials, systems and methods

We require information from authors about some types of materials, experimental systems and methods used in many studies. Here, indicate whether each material, system or method listed is relevant to your study. If you are not sure if a list item applies to your research, read the appropriate section before selecting a response.

Materials & experimental systems

n/a	Involved in the study
☐	☒ Antibodies
☒	☐ Eukaryotic cell lines
☒	☐ Palaeontology
☐	☒ Animals and other organisms
☒	☐ Human research participants
☒	☐ Clinical data

Methods

n/a	Involved in the study
☒	☐ ChIP-seq
☒	☐ Flow cytometry
☒	☐ MRI-based neuroimaging

Antibodies

Antibodies used

antibodies supplier catalog number
Rabbit Polyclonal Anti-GFP Thermo Fisher Scientific Cat# A11122
Rat Monoclonal Anti-GFP Nacalai Cat# 04404-84
Chicken Polyclonal Anti-GFP Thermo Fisher Scientific Cat# A10262
Rabbit Polyclonal Anti-Mouse CAR Millipore Cat# AB15282
Mouse Monoclonal Anti-Primate/Human CAR 7G6 Zhang et al., 2003
Goat Polyclonal Anti-ChAT Millipore Cat# AB144P
Mouse Monoclonal Anti-CRALBP Abcam Cat# ab15051
Rabbit Polyclonal Anti-RFP Rockland Cat#600-410-379
Guinea Pig Polyclonal Anti-RBPMS PhosphoSolutions Cat# 1832-RBPMS
Mouse Monoclonal Anti-Mouse Parvalbumin Millipore Cat# MAB1572
Rat Monoclonal Anti-Glycine ImmunoSolutions Cat# IG1002
Mouse Monoclonal Anti-Glutamine Synthetase (GS) Millipore Cat# MAB302
Mouse Monoclonal Anti-Tyrosine Hydroxylase (TH) Millipore Cat# MAB318
Alexa Fluor 488 donkey anti-rabbit IgG (H+L) Thermo Fisher Scientific Cat# A21206
Alexa Fluor 568 donkey anti-rabbit IgG (H+L) Thermo Fisher Scientific Cat#A10042
Alexa Fluor 647 donkey anti-rabbit IgG (H+L) Thermo Fisher Scientific Cat# A31573
Alexa Fluor 488 donkey anti-rat IgG (H+L) Thermo Fisher Scientific Cat# A21208
Alexa488-conjugated donkey anti-chicken IgY Jackson Immuno Research Cat#703-545-155
Alexa Fluor 488 donkey anti-mouse IgG (H+L) Thermo Fisher Scientific Cat# A21202
Alexa Fluor 555 donkey anti-mouse IgG (H+L) Thermo Fisher Scientific Cat# A31570
Alexa Fluor 647 donkey anti-mouse IgG (H+L) Thermo Fisher Scientific Cat# A31571
Alexa Fluor 488 donkey anti-goat IgG (H+L) Thermo Fisher Scientific Cat# A11055
Alexa Fluor 568 donkey anti-goat IgG (H+L) Thermo Fisher Scientific Cat# A11057
Alexa Fluor 633 donkey anti-goat IgG (H+L) Thermo Fisher Scientific Cat# A21082

Donkey anti-guinea pig Cy3 Jackson Immuno Research Cat# 706-165-148

Validation

The specificity of the primary and secondary antibodies was validated by the manufacturers.
Validation profiles for all antibodies can be found using online database and RRID number:
Rabbit Polyclonal Anti-GFP RRID: AB_221569
Rat Monoclonal Anti-GFP RRID: AB_2313654
Chicken Polyclonal Anti-GFP RRID: AB_2534023
Rabbit Polyclonal Anti-Mouse CAR RRID: AB_1163387
Mouse Monoclonal Anti-Primate/Human CAR 7G6 Zhang et al., 2003
Goat Polyclonal Anti-ChAT RRID: AB_2079751
Mouse Monoclonal Anti-CRALBP RRID: AB_2269474
Rabbit Polyclonal Anti-RFP RRID:AB_2209751
Guinea Pig Polyclonal Anti-RBPMS RRID: AB_2492226
Mouse Monoclonal Anti-Mouse Parvalbumin RRID: AB_2174013
Rat Monoclonal Anti-Glycine RRID: AB_10013222
Mouse Monoclonal Anti-Glutamine Synthetase (GS) RRID: AB_2110656
Mouse Monoclonal Anti-Tyrosine Hydroxylase (TH) RRID: AB_2201528
Alexa Fluor 488 donkey anti-rabbit IgG (H+L) RRID: AB_141708
Alexa Fluor 568 donkey anti-rabbit IgG (H+L) RRID:AB_2534017
Alexa Fluor 647 donkey anti-rabbit IgG (H+L) RRID: AB_2536183
Alexa Fluor 488 donkey anti-rat IgG (H+L) RRID: AB_141709
Alexa488-conjugated donkey anti-chicken IgY RRID:AB_2340375
Alexa Fluor 488 donkey anti-mouse IgG (H+L) RRID: AB_141607
Alexa Fluor 555 donkey anti-mouse IgG (H+L) RRID: AB_2536180
Alexa Fluor 647 donkey anti-mouse IgG (H+L) RRID: AB_162542
Alexa Fluor 488 donkey anti-goat IgG (H+L) RRID: AB_2534102
Alexa Fluor 568 donkey anti-goat IgG (H+L) RRID: AB_142581
Alexa Fluor 633 donkey anti-goat IgG (H+L) RRID: AB_141493
Donkey anti-guinea pig Cy3 RRID: AB_2340460

Animals and other organisms

Policy information about studies involving animals; ARRIVE guidelines recommended for reporting animal research

Laboratory animals

Mus musculus, C57BL/6J, male and female, age 6-8 weeks
Macaca fascicularis, male and female, age 5-19 years

Wild animals

The study did not involve wild animals.

Field-collected samples

The study did not involve samples collected from the field.

Ethics oversight

For mouse experiments:
European Communities Guidelines on the Care and Use of Laboratory Animals
For Non-human primate experiments:
Association for Assessment and Accreditation of Laboratory Animal Care, European Directive 2010/63 and the French National Charter on the Ethics of Animal Experimentation. All animal protocols were approved by the Institutional Animal Care and Use Committee of KBI or the French Ministry of Higher Education and Research (APAFIS#5716-2016061714424948v3)
For human retina tissue:
tissue samples were obtained in accordance with the tenets of the Declaration of Helsinki and protocols were approved by the local Hungarian ethics committees.

Note that full information on the approval of the study protocol must also be provided in the manuscript.